Practical Mechanically Interlocked Molecules: A Model of Gas Adsorption in Metal Organic Frameworks Harboring Rotaxane Molecular Shuttles

Jonathan Daniel Carney

An undergraduate thesis advised by David Roundy and Cory Simon
submitted to the Department of Physics, Oregon State University
in partial fulfillment of the requirements for the degree BSc in Physics
Submitted on May 5, 2020

Abstract

Metal organic frameworks(MOFs) are a class of crystalline materials utilized in gas storage, chemical sensing, and other engineering applications. Recently chemists have begun synthesizing MOFs with moving parts in order to further these applications. A wide array of dynamic MOFs have been created and theorized. Among them is the interlocking of a ring shaped molecule on the dumbbell like strut of a metal organic framework called a rotaxane molecular shuttle. Recently a rotaxane molecular shuttle(RMS) MOF was synthesized for the first time. This RMS-MOF is called UWDM-4 and is a proof of concept material for a mechanically interlocked molecule MOF with a moving shuttle harbored in its pores. In order to motivate further synthesization and experimentation with RMS-MOFs we pose a statistical mechanical model based on the langmuir model of gas adsorption that models the potential for both the shuttle-gas competition for binding sites and the entropic effects of the moving shuttle to affect gas adsorption. Our model is advantageous in that it can be solved analytically while allowing the two aforementioned effects to be explored. We defined a usable space of parameters for our model we termed material space, consisting of the bonding energies of the gas at two discrete stations on the strut of the MOF, and an energetic penalty for the rotaxane to occupy one of the binding sites(this allows us to model the shuttle favoring one side). We then compared adsorption properties to a single site MOF with the same expected gas occupancy at a given temperature. We found that an RMS-MOF located properly in material space to be less temperature sensitive to adsorption and to have a smaller heating effect from gas adsorption. Both allow for more efficacious gas storage.

Contents

1 Introduction **4**

1.1 MOFs for gas storage 4

1.2 Incorporating Rotaxane to speed Deadsorption 5

2 Theory **7**

2.1 Abstracting the RMS-MOF 7

2.2 Two mesostates at fixed n, T 9

2.2.1 The empty RMS-MOF 9

2.2.2 The gas-filled RMS-MOF 10

2.3 The ideal lattice gas 11

2.4 The single-□-site Langmuir model 12

2.4.1 Fixed $n \in \{0, 1\}, T$ models 13

2.5 RMS-MOF, Langmuir comparison 14

2.5.1 Defining a controlled comparison 14

2.5.2 Relationship between temperature-sensitivity of $\langle n \rangle$ and of the Henry coefficient, $K\beta$. 14

2.5.3 The ratio of adsorption sensitivities to temperature changes 14

2.5.4 The difference of adsorption sensitivities to temperature changes 15

2.5.5 Conditions for $S_{n=1} > S_{n=0}$ 15

2.6 β-sensitivity of $\langle n \rangle$ at isobar is $\beta\mu$-sensitivity of $\langle U \rangle$ at isotherm 16

3 Results **17**

3.1 The RMS-MOF immersed in gas at fixed μ, T 17

3.1.1 The gas adsorption isotherm 18

3.1.2 The position of the wheel 19

3.1.3 The energy change upon gas adsorption 21

3.2 Comparison to a single-site Langmuir model 24

3.2.1 Temperature-sensitivity of adsorption 24

3.2.2 Heat released upon adsorption 27

3.2.3 Summary 29

4 Discussion of results and directions for future research **30**

4.1 Discussion of results 30

4.2 directions for future research 31

List of Figures

1 RMS-MOF Model 7

2 Entropy as a Function of Expected Ring Position 17
3 Adsorption Isotherm of RMS-MOF 19
4 Tunability of Ring Position Pressure and Temperature Dependence 20
5 Empty to Saturated MOF Transition 22
6 Comparable Langmuir MOF 23
7 RMS vs Langmuir MOF Temperature Sensitivity 26
8 RMS vs Langmuir Heating Upon Adsorption 28

List of Tables

1 Microstates of RMS-MOF 8
2 Langmuir MOF 13
3 Description of model parameters/variables 18

1 Introduction

1.1 MOFs for gas storage

Much of modern gas storage is dependent on storing large amounts of gas at higher than atmospheric pressure in rigid pressure resistant containers. The primary method of extracting gas from such a system is to use pressure differences between the inside and outsides of such containers. In order for this process to occur at an efficient speed, it is often necessary for this pressure differential to be significant. This opens the door to potentially dangerous accidents driven by the containment of reactive gases at high pressures. One such example would be the containment of methane on board natural gas powered vehicles. These vehicles have the potential to bridge the gap between current fossil fuel vehicles and electric vehicles. Methane burns cleaner than traditional fossil fuels and is more readily available. However modern methane powered vehicles suffer from the need to carry heavy, pressure resistant gas tanks on board in order to carry adequate amounts of fuel. These tanks also tend to only be constructed in resilient shapes such as cylinders, restricting engineers from utilizing more advantageously shaped tanks utilized in gasoline powered vehicles. The most direct way to overcome these challenges is to reduce the necessary pressures within the gas storage tanks without sacrificing the ability to store gas or remove gas form the tank.

In order to meet this ambitious goal chemical engineers began developing alternatives to an empty tank. Usually this entails filling the tank with some sort of porous materials such as metal organic frameworks (MOFs)[29]. MOFs are a class of porous crystalline materials consisting of a lattice organic struts linking metallic nodes[63, 27]. MOFs can be synthesized so that they feature functional groups that attract gas molecules, this force of attraction can overcome the repulsive forces between gas molecules, placing them closer to one another than they would normally be packed at a given pressure[45]. This enables much larger amounts of gas to be stored at a given pressure, solving the first of the two challenges presented in increasing the efficacy of gas storage techniques. However this in turns makes removing gas from a MOF more complicated, gas molecules are attracted to a MOF and therefore are less likely to leave the tank at a given pressure. Fortunately MOFs are extremely tunable, owing to the wide variety of modular components that can be interchanged to create new MOFs. Thus far, tens of thousands of MOFs have been synthesized[44] and tens of thousands more have been theorized. This versatile adjustability allows one to tune the chemistry of MOFs to target specific properties. In addition to this inherent adjustability, MOFs possess large surface areas from their porosity[26]. This makes MOFs useful in a diverse array of engineering applications such as the aforementioned gas storage [45], gas separations [39, 6], and sensing [36, 64]. This tenability can potentially overcome this challenge by enabling engineers to synthesize MOFs with dynamic or flexible compounds integrated into their structure[18]. Flexible MOFs have been synthesized extensively for this purpose[31, 48, 16, 12, 38] giving rise to various anomalous adsorption properties that deviate from the behavior of more structurally simple MOFs in manners that have useful applications in gas storage.

Modes of flexibility include the rotation of ligands [61], hinge motion of wine-rack-like backbones [49, 13, 43], and displacement of interdigitated or interpenetrated networks [32]; consequent anomalous adsorption

properties [17] include inflections [21] and discontinuities [48] in gas adsorption isotherms, intrinsic mitigation of the heat released upon adsorption [43], negative gas adsorption [35], adsorption-induced contraction [8] and expansion [43], metastability [28, 22], and adsorption/desorption hysteresis [13]. In addition to benefits for gas storage, such gas-induced framework expansion could be leveraged for stress-based gas sensors [2].

Dynamic MOFs have been shown to more easily expel stored gas and the dynamic qualities of some consume a fraction of the heat released upon adsorption [10]. Both of these properties give them the potential to outperform rigid MOFs in gas storage applications by more easily adsorbing and deadsorbing gas with response to change in temperature. However, despite their appealing adsorption properties, MOFs with pliable struts and backbones are arguably infeasible for practical applications: repeated dynamics eventually lead to structural failure and degradation [18].

1.2 Incorporating Rotaxane to speed Deadsorption

One possible way to get around the inevitable structure degradation of MOFs with dynamic properties while still maintaining exotic adsorption properties that may assist in engineering applications is to graft movable interlock molecules to the struts of a rigid MOF [18, 14, 46]. In contrast to MOFs with pliable struts and backbones which, subject to repeated dynamics, will rupture, mechanically interlocked molecules [55, 9] can undergo repeated dynamics without breakage. This solves our problem that arose with flexible MOFs, and with the correct choice of interlocked molecules we can still respond to exotic external stimuli such as an electric field [14]. Dynamic MOFs have the potential to offer a solution to our engineering problem, allowing a MOF to be emptied by applying stimulus via heat, electric fields, or other stimuli while also being robust enough to work for many duty cycles.

As an example mechanically interlocked molecule, is [2]rotaxane [3, 5, 14, 1] which consists of a long molecule (the "axle") threaded through a ring shaped molecule called a macrocycle (the "wheel"); bulky groups at the two ends of the axle prevent the wheel from sliding off, thereby mechanically interlocking the wheel and axle. In a [2]rotaxane *molecular shuttle*, the wheel translates along the axle, which can feature bonding sites that serve as "stations" for the wheel, possibly with different affinities for it. These bonding sites may just be energetic minima along the axle for the macrocyclic ring, however for our purposes we can treat these stations as discrete bonding sites. Figure 1 provides a useful depiction of this model. Experimental studies have demonstrated the integration of rotaxanes [40, 65, 15, 25, 59, 66, 60, 41, 33, 4] into MOF scaffolds, but resultant adsorption properties have not been investigated.

Metal-organic frameworks with rotaxane molecular shuttles operating in their pores have been synthesized [65] and offer a potential solution to the search for MOFs that can drive off gas more effectively than non-dynamic MOFs while also retaining their structural integrity. In these MOFs an change in total system temperature would be the stimulus that would drive gas out of the MOF. The presence of the shuttling wheel may potentially affect adsorption and deadsorption via both energetic and entropic effects. Energetic effects could involve the wheel and gas competing for bonding sites, changing the affinity of the gas for the MOF, while potential entropic effects involve the thermal effect of the shuttling wheel. In 2015, Loeb and

coworkers [65] synthesized an rotaxane molecular shuttle MOF (RMS-MOF) coined UWDM-4 [46]. The struts of UWDM-4 serve as the axle for a [2]rotaxane, whose macrocyclic wheel was shown to rapidly shuttle between two benzimidazole stations on its strut, unimpeded owing to the porosity of the MOF [65]. Gas adsorption was not investigated, but UWDM-4 provides a proof of concept justifying further investigation into RMS-MOFs for a diversity of applications.

The goal of this thesis project is to produce a simple statistical mechanical model based on UWDM-4 in hopes of finding advantageous adsorption and deasdsorption behavior in comparison to a simpler, rigid metal organic framework. Advantageous or anomalous behavior (in this model) might potentially arise from entropic effects due to the shuttling of the wheel and competition between the wheel and gas for bonding sites. If this model is successful in showing such behavior it will hopefully provide an impetuous to future research on the use of MIMs in gas storage.

2 Theory

2.1 Abstracting the RMS-MOF

In order to understand the gas adsorption behavior of an RMS-MOF on a realistic scale we will pose a simple statistical mechanical model based on a few simplifying assumptions. Our primary goal with this model is to produce an analytically solvable model of a RMS-MOF that will illuminate potential anomalous gas adsorption properties when compared to a static MOF. We will base our model on the Langmuir model of gas adsorption [56].

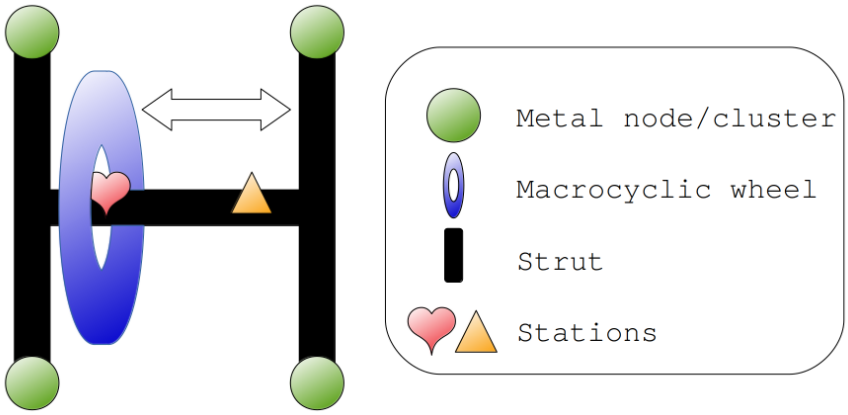

Figure 1: Our abstraction of the unit cell of a MOF with a rotaxane molecular shuttle operating in its pores, an RMS-MOF. The wheel can translate along the rotaxane axle (the strut of the MOF), which harbors two distinct stations ($\heartsuit$ and $\triangle$) for the wheel that also serve as adsorption sites for a gas molecule. If the wheel occupies the $\heartsuit$ ($\triangle$) station, the $\triangle$ ($\heartsuit$) adsorption site is exposed to the gas.

Our hope in utilizing a simple model in hopes of discovering interesting gas adsorption behaviors is that might inspire future, more complex work. With this motivation we pose the model seen in figure 1. Our two site model is inspired by UWDM-4 [65], with the added assumption that the ring prefers one bonding site over the other(the $\heartsuit$ station). The rotaxane is able to move along the strut of the MOF it is linked with and occupies one of the two available gas bonding stations at any given time. This leaves a single gas adsorption site available. In some MOFs the structure can shift due to factors such as pressure, temperature, electromagnetic fields, or gas adsorbed. We will assume that the structure of the RMS-MOF is rigid, and therefore our model is assumed to be invariant under any external changes to the system.

This simplified model will constrain our system to one of two microstates when gas is absent from the system and one of four available microstates when the RMS-MOF is immersed in gas. Because we have chosen an interaction-less model we are able to treat the MOF as a collection of arbitrarily many of these unit cells, each in it's own microstate. In order to denote the micro states we will use the following, let $r \in \{0,1\} \equiv \mathcal{R}$ denote the state of the macrocyclic wheel on the strut ($r = 0 \implies$ wheel on $\heartsuit$, $r = 1 \implies$ wheel on $\triangle$) and $n \in \{0,1\} \equiv \mathcal{N}$ denote the number of adsorbed gas molecules in the unit cell.

In order for our statistical mechanical model to be useful we will need to know the potential energy of

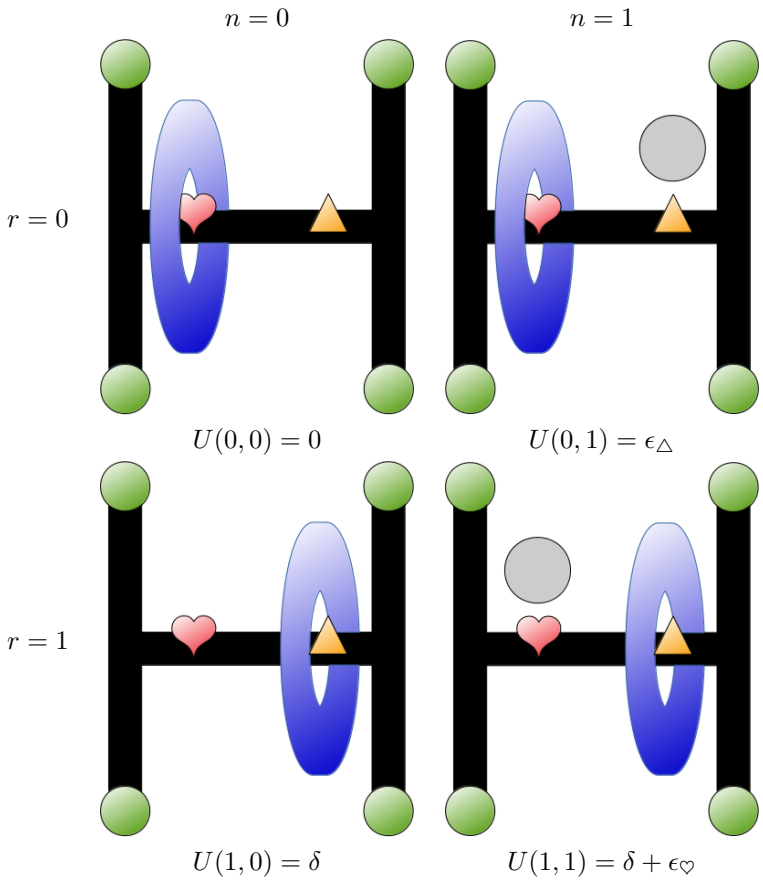

Table 1: List of microstates for a RMS-MOF-gas system and their potential energies. Gray sphere represents an adsorbed gas molecule.

each possible microstate. As mentioned before we distinguish the ♡ station as the one preferred by the rotaxane, in order to address this preference there will be an energetic penalty δ for the rotaxane to occupy the △ station. When a gas molecule is bonded at a station will experience a potential energy due interactions with the site. We will denote these potentials as $\epsilon_{\heartsuit}$ and $\epsilon_{\triangle}$. We will refer to the multitude of the potential combinations of these three parameters henceforth as material space, with a certain selection of the three being a point in material space. In order to have each point in material space correspond to a unique synthesis of an RMS-MOF we will constrain $\delta \geq 0$. Because repulsive adsorption sites would be of very little use to us, we will also only consider cases$\epsilon_{\triangle}, \epsilon_{\heartsuit} < 0$, or materials in which both adsorption sites are attractive to gas molecules. Tab. 3 summarizes model parameters and variables. We will draw no distinction between different types of gas molecules in our model, nor consider their interactions with one another.

With all of this considered, the potential energy U of the RMS-MOF-gas microstate (r, n) can be written as:

$$U(r, n) = r\delta + n[r\epsilon_{\heartsuit} + (1 - r)\epsilon_{\triangle}]. \tag{1}$$

2.2 Two mesostates at fixed n, T

The two by two nature of this model is very convenient as it allows us to employ a technique called coarse graining. Coarse graining describes the system with mesostates, somewhere between a micro and a macro state. These are not the smallest possible set states we are used to in statistical mechanics, nor are they full brown macroscopic properties. Rather they are an analytical tool that will prove fruitful. Particularly we will examine the behavior of the system when the RMS-MOF is empty($n = 1$) and then when the system is saturated (n=0).

2.2.1 The empty RMS-MOF

We'll begin with the empty two state model. In this case we are exploring the left column of Tab. 1. When the RMS-MOF unit cell is empty of gas, it behaves as a two-state model under the Canonical ensemble, toggling between the $(r = 0, n = 0)$ and $(r = 1, n = 0)$ microstates with energy 0 and δ, respectively. The $n = 0$ Canonical partition function of the empty(no gas) RMS-MOF unit cell is:

$$q_{n=0}(T) = \sum_{\mathcal{R}} e^{-\beta U(r,0)} = 1 + e^{-\beta\delta}, \tag{2}$$

where $\beta = 1/(k_{\mathrm{B}}T)$ with k_{B} the Boltzmann constant. The first and second terms correspond to the $(r = 0, n = 0)$ and $(r = 1, n = 0)$ microstates, respectively.

The expected value of r, which is the probability that the wheel occupies the △ station, is:

$$\langle r \rangle_{n=0}(T) = \frac{e^{-\beta\delta}}{1 + e^{-\beta\delta}}. \tag{3}$$

As the energetic penalty δ increases, the wheel becomes less likely to occupy the △ station. The wheel becomes more likely to occupy the △ station– the higher-energy microstate– as temperature increases, with $\langle r \rangle_{n=0} \to \frac{1}{2}$ as $T \to \infty$.

The expected energy is δ weighted by the probability that the wheel occupies the $\triangle$ station:

$$\langle U\rangle_{n=0}(T) = \delta\langle r\rangle_{n=0}(T). \tag{4}$$

Finally, the entropy is:

$$S_{n=0}(T) = -k_{\mathrm{B}}\Big[\langle r\rangle_{n=0}(T)\log\left[\langle r\rangle_{n=0}(T)\right] + \left[1-\langle r\rangle_{n=0}(T)\right]\log\left[1-\langle r\rangle_{n=0}(T)\right]\Big], \tag{5}$$

which is maximal when the wheel has no preference for a station ($\delta = 0$) and both microstates are equally probable.

2.2.2 The gas-filled RMS-MOF

Next we will address the more complicated, but more interesting two state model of a saturated RMS-MOF(right column of Tab. 1). When the RMS-MOF unit cell is occupied by a gas molecule, it behaves as a two-state model, toggling between the $(r = 0, n = 1)$ and $(r = 1, n = 1)$ microstates with energy $\epsilon_{\triangle}$ and $\delta + \epsilon_{\heartsuit}$, respectively. The $n = 1$ Canonical partition function of the RMS-MOF unit cell is:

$$q_{n=1}(T) = \sum_{\mathcal{R}} e^{-\beta U(r,1)} = e^{-\beta\epsilon_{\triangle}} + e^{-\beta(\epsilon_{\heartsuit}+\delta)}. \tag{6}$$

The first and second terms correspond to the $(r = 0, n = 1)$ and $(r = 1, n = 1)$ microstates, respectively; if the wheel occupies the $\triangle$ station, the gas must occupy the $\heartsuit$ adsorption site, and vice versa.

Because the canonical ensemble for this mesostate depends on all three parameters of material space, whereas the $n = 0$ mesostate depended only on δ, the behavior is much more chemically tunable.

If the gas prefers the $\triangle$ site or if the preference of the gas for the $\heartsuit$ site is less than that of the wheel ($\epsilon_{\triangle} < \epsilon_{\heartsuit} + \delta$), the wheel sits at the $\heartsuit$ station in the minimum-energy microstate—as in the $n = 0$ case. On the other hand, if the preference of the gas for the $\heartsuit$ site is greater than that of the wheel ($\epsilon_{\heartsuit} + \delta < \epsilon_{\triangle}$), the wheel sits at the $\triangle$ station in the minimum-energy microstate—opposite of the $n = 0$ case. Because a thermal system populates higher energy microstates at higher temperatures, we will find that temperature increases affect the position of the wheel differently depending on the sign of $\epsilon_{\triangle} - (\epsilon_{\heartsuit} + \delta)$.

The probability that the wheel occupies the $\triangle$ station is:

$$\langle r\rangle_{n=1}(T) = \frac{1}{1 + e^{-\beta[\epsilon_{\triangle} - (\epsilon_{\heartsuit}+\delta)]}}. \tag{7}$$

As in the $n = 0$ case, the wheel becomes less likely to occupy the $\triangle$ station as the energetic penalty δ increases. We also see the effect of the gas competing with the wheel for the stations: as the energy of interaction of the gas with the $\heartsuit$ ($\triangle$) site decreases (i.e., as the interaction becomes more favorable), the wheel becomes less likely to occupy the $\heartsuit$ ($\triangle$) station. The quantity $\epsilon_{\triangle} - (\epsilon_{\heartsuit} + \delta)$ describes the degree that the gas competes with the wheel for the $\heartsuit$ station, and its sign dictates whether the wheel occupies the $\heartsuit$ or $\triangle$ station in the minimum-energy microstate. Consequently, temperature changes have a different effect on the wheel in the gas-filled RMS-MOF depending on how $\epsilon_{\triangle}$ and $\epsilon_{\heartsuit} + \delta$ compare. If $\epsilon_{\triangle} = \epsilon_{\heartsuit} + \delta$, temperature changes have no effect on the wheel since both microstates have equal energy. If $\epsilon_{\triangle} < \epsilon_{\heartsuit} + \delta$, increasing

temperature induces the wheel to occupy the △ station more. If $\epsilon_{\heartsuit} + \delta < \epsilon_{\triangle}$, increasing temperature induces the wheel to occupy the ♡ station more.

The expected energy is the sum of the energies of the two microstates weighted by their probability of occurrence:

$$\langle U \rangle_{n=1}(T) = (\epsilon_{\heartsuit} + \delta)\langle r \rangle_{n=1}(T) + \epsilon_{\triangle}\left[1 - \langle r \rangle_{n=1}(T)\right]. \tag{8}$$

Finally, the entropy has the same form as we saw for the $n = 0$ case when expressed in terms of $\langle r \rangle_{n=1}$:

$$S_{n=1}(T) = -k_{\mathrm{B}}\Big[\langle r \rangle_{n=1}(T)\log[\langle r \rangle_{n=1}(T)] + [1 - \langle r \rangle_{n=1}(T)]\log[1 - \langle r \rangle_{n=1}(T)]\Big] \tag{9}$$

which is maximal when the $(r = 0, n = 1)$ and $(r = 1, n = 1)$ microstates have equal energy (when $\epsilon_{\triangle} = \epsilon_{\heartsuit} + \delta$) and thus occur with equal probability. Another important case is when $S_{n=0}(T) = S_{n=1}(T)$, which occurs when either $\epsilon_{\triangle} = \epsilon_{\heartsuit}$ or $\epsilon_{\triangle} = \epsilon_{\heartsuit} + 2\delta$. In each case, the magnitude of the energy difference between the two $n = 1$ states is δ, which is equal to the energy difference between the two $n = 0$ states.

2.3 The ideal lattice gas

Here, we derive properties of the ideal lattice gas from statistical thermodynamics.

Consider a lattice of M sites. The particles within an *ideal* lattice gas do not interact; thus, in addition to neglecting attractive forces between particles, we neglect repulsive forces and allow any number of particles to belong to a given lattice site. The canonical partition function $Q_{ig}(N, M, T)$ for an ideal gas lattice gas of N particles at temperature T is therefore:

$$Q_{ig}(N, M, T) = \frac{1}{N!}M^N, \tag{10}$$

since each particle can be independently assigned to belong to one of M lattice sites; we divide by $N!$ to treat the gas particles as indistinguishable. The chemical potential is a derivative of the Helmholtz free energy A, which we can write in terms of the Canonical partition function:

$$\mu_{ig} = \left(\frac{\partial A}{\partial N}\right)_{M,T} = -k_{\mathrm{B}}T\left(\frac{\partial \log Q_{ig}}{\partial N}\right)_{M,T}. \tag{11}$$

Applying Stirling's approximation for $N!$ and taking the derivative, we find the chemical potential for the ideal lattice gas is:

$$\mu_{ig} = k_{\mathrm{B}}T\log\left(\frac{N}{M}\right). \tag{12}$$

We next derive the ideal lattice gas law, which will allow us to replace density $\rho \equiv N/M$ in eqn. 12 with βP.

The pressure P of the gas is related to the Helmholtz free energy by:

$$P = -\left(\frac{\partial A}{\partial M}\right)_{N,T} = k_{\mathrm{B}}T\left(\frac{\partial \log Q_{ig}}{\partial M}\right)_{N,T} \tag{13}$$

Here, the number of lattice sites M plays the role of volume; as a consequence, the units of pressure in the lattice gas have units of energy. Taking the derivative of the partition function given by eqn. 10, we arrive at the ideal lattice gas law:

$$P = k_{\mathrm{B}}T\frac{N}{M}. \tag{14}$$

This shows that the density of the ideal lattice gas $\rho_{ig} \equiv N/M = \beta P$. Again, because P has units of energy, βP is unitless, which is consistent with the unitless density ρ. Combining eqn. 12 with eqn. 14, we arrive at:

$$\mu_{ig} = k_{\mathrm{B}} T \log(\beta P). \tag{15}$$

Eqn. 15 allows us to replace $e^{\beta\mu}$ in our RMS-MOF model under the grand-canonical ensemble with βP to relate to the more directly experimentally accessible quantity of pressure.

The ideal lattice gas model is a reasonable approximation of a gas only at low density and high temperature. Note that we (a) treat the bulk gas phase as ideal yet (b) restrict a lattice site in the RMS-MOF model in Fig. 1 to hold at most one gas molecule. This may seem inconsistent, but, the gas density in a RMS-MOF that offers attractive adsorption sites ($\epsilon_{\heartsuit}, \epsilon_{\triangle} < 0$) is greater than in the bulk gas phase with which the RMS-MOF is in thermodynamic equilibrium. Thus, in modeling the RMS-MOF immersed in the ideal lattice gas, neglecting gas-gas repulsive forces can be a reasonable approximation for the bulk gas phase yet unreasonable for the adsorbed phase inside the RMS-MOF, as the density is typically much greater in the adsorbed phase.

We did not specify the volume of the lattice sites, and the results in eqns. 12 and 14 are not explicitly dependent on the volume of each lattice site. Provided the volume of the lattice sites is chosen to be roughly the volume of the gas particle, the ideal lattice gas law deviates from a real gas when the condition $\rho = \beta P << 1$ does not hold.

2.4 The single-□-site Langmuir model

The unit cell of a single-□-site Langmuir material offers a single gas adsorption site, □, with adsorption energy $\epsilon_{\square}$. See Fig. 6a. Each adsorption site behaves independently of the other adsorption sites, and adsorbed gas molecules do not interact. In the following derivation of the adsorption properties of a single-□-site Langmuir material, we adopt the same notation for the RMS-MOF as in Tab. 3, but decorate variables/parameters with "L".

There are only two possible microstates in the single-□-site Langmuir model, one where the unit cell is empty ($n_L = 0$) and one where the unit cell is occupied by a gas molecule ($n_L = 1$). See Tab. 2. The potential energy of each microstate is given by:

$$U_L(n_L) = n_L \epsilon_{\square}, \tag{16}$$

for $n_L \in \{0, 1\}$.

Consider the unit cell of the single-□-site Langmuir material in thermodynamic equilibrium with a heat bath and particle bath consisting of an ideal gas at chemical potential μ and temperature T. The grand canonical partition function of the unit cell of the single-□-site Langmuir material in Fig. 6a is:

$$\xi_L(\mu, T) = 1 + e^{-\beta\epsilon_{\square}} e^{\beta\mu}. \tag{17}$$

The first and second terms correspond to $n_L = 0$ and $n_L = 1$, respectively. Following eqn. 46, we find the

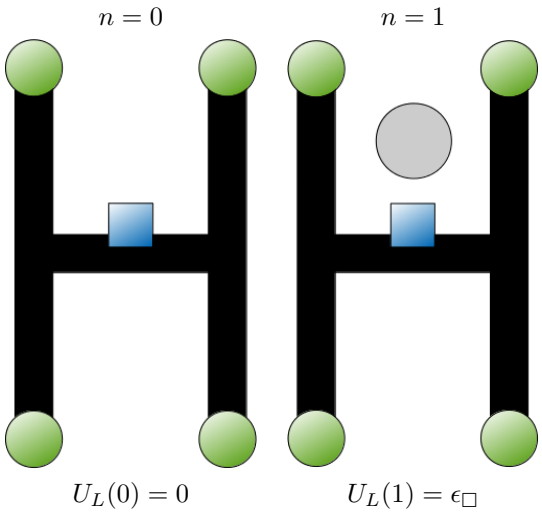

Table 2: List of microstates for a single-$\square$-site Langmuir model and their potential energies. Gray sphere represents an adsorbed gas molecule.

expected number of adsorbed gas molecules in the Langmuir material $\langle n_L \rangle$ as:

$$\langle n_L \rangle(P,T) = \left(\frac{\partial \log \xi_L}{\partial(\beta\mu)} \right)_\beta = \frac{K_L}{1 + K_L \beta P} \beta P, \tag{18}$$

where the Langmuir constant K_L is a function of temperature and the interaction of the gas with the $\square$ adsorption site, $\epsilon_\square$:

$$K_L(T) = e^{-\beta \epsilon_\square}. \tag{19}$$

We again took the bulk gas to be an ideal lattice gas (see Sec. 2.3) to replace $e^{\beta\mu}$ with βP.

The average energy of the single-$\square$-site material-gas system is:

$$\langle U_L \rangle = -\left(\frac{\partial \log \xi_L}{\partial \beta} \right)_{\beta\mu} = \epsilon_\square \langle n_L \rangle. \tag{20}$$

Thus, the energy change upon adsorption is:

$$\left(\frac{\partial \langle U_L \rangle}{\partial \langle n_L \rangle} \right)_\beta = \epsilon_\square. \tag{21}$$

2.4.1 Fixed $n \in \{0, 1\}, T$ models

In the Langmuir model, there is only one microstate when either $n = 0$ or $n = 1$ is fixed; see Tab. 2. Thus:

$$S_{L,n=0} = S_{L,n=1} = 0. \tag{22}$$

The existence of only one microstate at fixed $n = 0$ or $n = 1$ also implies, trivially:

$$\langle U_L \rangle_{n=0} = 0 \tag{23}$$

$$\langle U_L \rangle_{n=1} = \epsilon_\square. \tag{24}$$

The Helmholtz free energies of the fixed $n = 0$ and $n = 1$ states are then:

$$A_{L,n=0} = 0 \tag{25}$$

$$A_{L,n=1} = \epsilon_{\square}, \tag{26}$$

since $A_L = \langle U_L \rangle - TS_L$.

Now note that we can write K_L in eqn. 19 in terms of the free energy change upon gas adsorption:

$$K_L(T) = e^{-\beta(A_{L,n=1} - A_{L,n=0})}, \tag{27}$$

which is the analogy of eqn. 48 for the psuedo-Langmuir constant of the RMS-MOF.

2.5 RMS-MOF, Langmuir comparison

In this section, we compare an RMS-MOF to a single-$\square$-site Langmuir model. We define the temperature-sensitivity of a variable X as $\left(\frac{\partial X}{\partial T}\right)_P$. We inspect the ratio of and difference between the temperature-sensitivities of adsorption in the RMS-MOF and Langmuir models.

2.5.1 Defining a controlled comparison

For a controlled comparison, we set the interaction of the gas with the $\square$ adsorption site, $\epsilon_{\square}$, such that the Langmuir constant is equal to the pseudo-Langmuir constant of the RMS-MOF at some temperature T_0, i.e. we tune the Langmuir material to impose $K_L(T_0) = K(T_0)$. This ensures that the RMS-MOF and Langmuir materials possess identical adsorption isotherms at temperature T_0, via comparing eqns. 46 and 18. Throughout this section, we take $K_L(T_0) = K(T_0)$.

2.5.2 Relationship between temperature-sensitivity of $\langle n \rangle$ and of the Henry coefficient, $K\beta$

By the chain rule:

$$\left(\frac{\partial \langle n \rangle}{\partial T}\right)_P = \left(\frac{\partial \langle n \rangle}{\partial (K\beta P)}\right)_P \left(\frac{\partial (K\beta P)}{\partial T}\right)_P. \tag{28}$$

The quantity $\left(\frac{\partial \langle n \rangle}{\partial (K\beta P)}\right)_P$ follows from $\langle n \rangle$ in eqn. 46, and the P can be factored out of the derivative on the right, giving us:

$$\left(\frac{\partial \langle n \rangle}{\partial T}\right)_P = \frac{1}{(1 + K\beta P)^2} P \frac{\partial (K\beta)}{\partial T} \tag{29}$$

At dilute conditions, $\langle n \rangle \approx K\beta P$; $K\beta$ is the Henry coefficient. Therefore, eqn. 29 relates the temperature-sensitivity of the Henry coefficient to that of $\langle n \rangle$ at any pressure. Because the Langmuir model possesses an identical adsorption isotherm, the analogy of eqn. 29 holds for n_L and K_L.

2.5.3 The ratio of adsorption sensitivities to temperature changes

The *ratio* of the temperature sensitivities of $\langle n \rangle$ and $\langle n_L \rangle$ at any pressure is equal to the ratio of the temperature sensitivities of the Henry coefficients:

$$K(T_0) = K_L(T_0) \implies \frac{\left(\frac{\partial \langle n \rangle}{\partial T}\right)_P}{\left(\frac{\partial \langle n_L \rangle}{\partial T}\right)_P} = \frac{\frac{\partial (K\beta)}{\partial T}}{\frac{\partial (K_L\beta)}{\partial T}} \text{ at } T_0. \tag{30}$$

This follows from applying eqn. 29.

2.5.4 The difference of adsorption sensitivities to temperature changes

We now inspect the *difference* in temperature-sensitivity of the Henry coefficients. The product rule

$$\frac{\partial(K\beta)}{\partial T} = \frac{1}{k_{\mathrm{B}}T}\frac{\partial K}{\partial T} - \frac{1}{k_{\mathrm{B}}T^2}K \tag{31}$$

implies that the difference in temperature-sensitivities of the Henry coefficients is related to the difference in temperature-sensitivities of the pseudo-Langmuir and Langmuir constants:

$$K(T_0) = K_L(T_0) \implies \frac{\partial(K\beta)}{\partial T} - \frac{\partial(K_L\beta)}{\partial T} = \frac{1}{k_{\mathrm{B}}T}\left(\frac{\partial K}{\partial T} - \frac{\partial K_L}{\partial T}\right) \text{ at } T_0. \tag{32}$$

The temperature-sensitivity of K is:

$$\frac{\partial K}{\partial T} = K\frac{\partial}{\partial T}\left[\frac{1}{k_{\mathrm{B}}T}(A_{n=0} - A_{n=1})\right] \tag{33}$$

$$\frac{\partial K}{\partial T} = K\left[-\frac{1}{k_{\mathrm{B}}T^2}(A_{n=0} - A_{n=1}) + \frac{1}{k_{\mathrm{B}}T}\left(\frac{\partial A_{n=0}}{\partial T} - \frac{\partial A_{n=1}}{\partial T}\right)\right] \tag{34}$$

$$\frac{\partial K}{\partial T} = \frac{K}{k_{\mathrm{B}}T}\left[-\frac{1}{T}(A_{n=0} - A_{n=1}) - (S_{n=0} - S_{n=1})\right] \tag{35}$$

The first line follows from eqn. 47. The second line follows from the product rule. The third line follows from the the thermodynamic identity $dA = -SdT - PdV + \mu dN$.

Since the analogy of eqn. 47 holds for the single-site Langmuir model as well (see eqn. 27):

$$K(T_0) = K_L(T_0) \implies A_{n=1} - A_{n=0} = A_{L,n=1} - A_{L,n=0} \text{ at } T_0 \tag{36}$$

That is, if the single-site Langmuir model and RMS-MOF model exhibit an identical adsorption isotherm at temperature T_0, the free energy difference between the $n = 1$ and $n = 0$ states must be equal among the two materials at temperature T_0.

Combining eqns. **??** and 36:

$$K(T_0) = K_L(T_0) \implies \frac{\partial K}{\partial T} - \frac{\partial K_L}{\partial T} = \frac{K}{k_{\mathrm{B}}T}\left(S_{n=1} - S_{n=0}\right) \text{ at } T_0 \tag{37}$$

The latter follows from eqn. 22.

Finally, combining eqns. 37 and 32:

$$K(T_0) = K_L(T_0) \implies \frac{\partial(K\beta)}{\partial T} - \frac{\partial(K_L\beta)}{\partial T} = \frac{K}{(k_{\mathrm{B}}T)^2}\left(S_{n=1} - S_{n=0}\right) \text{ at } T_0. \tag{38}$$

We have arrived at the difference of the temperature-sensitivities of the Henry coefficients of the RMS-MOF and Lanmguir models.

2.5.5 Conditions for $S_{n=1} > S_{n=0}$

If the addition of a gas molecule to the RMS-MOF unit cell increases the entropy of the RMS-MOF system in Fig. 1, i.e. if $S_{n=1} > S_{n=1}$, then, according to eqns. 54 and 57:

- adsorption in the RMS-MOF is less temperature-sensitive than in the single-site Langmuir model with an identical adsorption isotherm at T_0
- the heat released upon adsorption in the RMS-MOF is less than in the single-site Langmuir model with an identical adsorption isotherm at T_0.

Here, we derive which regions in RMS-MOF material space $(\delta, \epsilon_\heartsuit, \epsilon_\triangle)$ satisfy $S_{n=1} > S_{n=0}$ and thus lead to this behavior.

Fig. 2 depicts the entropy of the RMS-MOF-gas system at fixed $n \in \{0, 1\}$ as a function of the probability that the wheel occupies the $\triangle$ station, $\langle r \rangle_{n=0,1}$. Both $S_{n=0}$ and $S_{n=1}$ are identical functions of $\langle r \rangle_{n=0}$ and $\langle r \rangle_{n=1}$, respectively; see eqns. 5 and 9. Depicted by the red region in the plot, we geometrically see:

$$S_{n=1} > S_{n=0} \iff \langle r \rangle_{n=0} < \langle r \rangle_{n=1} < 1 - \langle r \rangle_{n=0}. \tag{39}$$

Applying eqns. 5 and 9, we find the constraints on RMS-MOF material parameter space to be:

$$S_{n=1} > S_{n=0} \iff \epsilon_\heartsuit < \epsilon_\triangle < \epsilon_\heartsuit + 2\delta. \tag{40}$$

This region of material space is the pink band in Fig. 7a and the orange band in Fig. 8.

In words, $S_{n=1} > S_{n=0}$ iff both (i) the gas-$\heartsuit$ interaction is more favorable than that of the gas-$\triangle$ interaction ($\epsilon_\heartsuit < \epsilon_\triangle$) and (ii) the gas-$\heartsuit$ and gas-$\triangle$ interaction energies do not differ by more than 2δ, i.e., the preference of the gas for the $\heartsuit$ station is limited ($\epsilon_\triangle < \epsilon_\heartsuit + 2\delta$). Because $\delta > 0$, condition (i) ensures that gas adsorption causes the wheel to occupy the $\heartsuit$ station less often (see Fig. 4), as gas will compete with the wheel for and thus to an extent exclude the wheel from the $\heartsuit$ station; this increases the entropy of the system provided that condition (ii) also holds. If condition (i) held but condition (ii) did not, the gas would exclude the wheel from the $\heartsuit$ station more than the penalty $\delta > 0$ excluded the wheel from the $\triangle$ station when the gas was absent, thereby reducing the entropy from $S_{n=0}$.

2.6 β-sensitivity of $\langle n \rangle$ at isobar is $\beta\mu$-sensitivity of $\langle U \rangle$ at isotherm

The β-sensitivity of $\langle n \rangle$ at fixed pressure (invoking the ideal lattice gas law, this is equivalent to fixed $\beta\mu$) is:

$$\left(\frac{\partial \langle n \rangle}{\partial \beta}\right)_{\beta\mu} = \left(\frac{\partial}{\partial \beta}\left(\frac{\partial \log \xi}{\partial(\beta\mu)}\right)_{\beta}\right)_{\beta\mu} \tag{41}$$

$$= \left(\frac{\partial}{\partial(\beta\mu)}\left(\frac{\partial \log \xi}{\partial \beta}\right)_{\beta\mu}\right)_{\beta} \tag{42}$$

$$= -\left(\frac{\partial \langle U \rangle}{\partial(\beta\mu)}\right)_{\beta} \tag{43}$$

The first line follows from eqn. 46. The second line follows from the mixed derivative theorem. The third line follows from writing the expected value of U as a derivative of the partition function. Using eqn. 46 and $\beta P = e^{\beta\mu}$ from the ideal lattice gas law, finally, we can relate temperature-sensitivity of adsorption to the energy change upon adsorption via a change in derivative:

$$\left(\frac{\partial \langle n \rangle}{\partial \beta}\right)_{\beta\mu} = -k_{\mathrm{B}}T^2\left(\frac{\partial \langle n \rangle}{\partial T}\right)_{\beta\mu} = -\langle n \rangle(1 - \langle n \rangle)\left(\frac{\partial \langle U \rangle}{\partial \langle n \rangle}\right)_{\beta}. \tag{44}$$

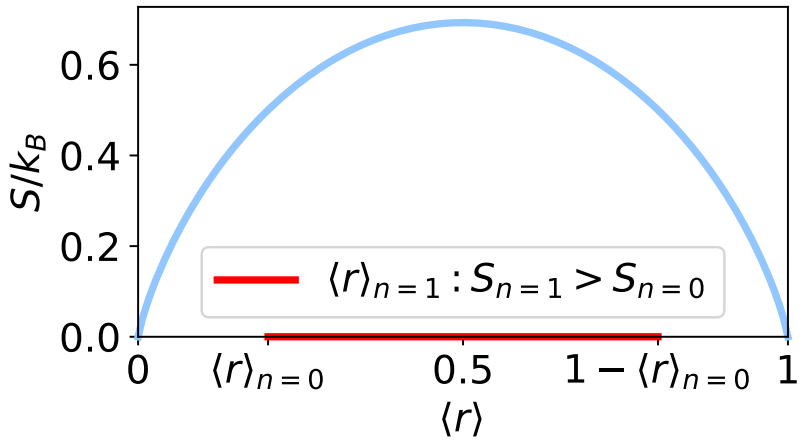

Figure 2: The entropy $S_{n=0,1}/k_{\mathrm{B}}$ as a function of $\langle r\rangle_{n=0,1}$, given in eqn. 5 or 9. Marked is a hypothetical value of $\langle r\rangle_{n=0}$ and the resulting $1-\langle r\rangle_{n=0}$. Because entropy is a measure of disorder, it follows that there will be maximal entropy when both states are equally probably. The red line depicts the range of values of $\langle r\rangle_{n=1}$ such that $S_{n=1} > S_{n=0}$.

3 Results

3.1 The RMS-MOF immersed in gas at fixed μ, T

Now that we have established the relevant theory we will use the grand-canonical ensemble to model the RMS-MOF when it is in a state of thermodynamic equilibrium with it's surroundings, a "bath" of pure gas with a known temperature(T) and chemical potential(μ). The chemical potential will be a function of the pressure of the gas, given by the ideal lattice gas derived in the theory section. Our goal is to determine the gas adsorption $\langle n\rangle$, state of the wheel $\langle r\rangle$, and expected energy $\langle U\rangle$ as a function of temperature, pressure, and material parameters. From these values we will be bale to infer the macroscopic behavior of the RMS-MOF. As each RMS-MOF unit cell in Fig. 1 is independent, $\langle n\rangle$ represents the fraction of unit cells in a macroscopic RMS-MOF crystal that are occupied by a gas molecule, and $\langle r\rangle$ represents the fraction of the wheels that occupy the $\triangle$ station.

We write the grand-canonical partition function ξ for the RMS-MOF unit cell in Fig. 1 in terms of the two Canonical partition functions in eqns. 2 and 6:

$$\begin{aligned}\xi(\mu,T) &= \sum_{\mathcal{R}\times\mathcal{N}} e^{-\beta U(r,n)+\beta\mu n} \\ &= q_{n=0}(T) + q_{n=1}(T)e^{\beta\mu}. \end{aligned} \tag{45}$$

In a sense, we have coarse-grained our model by agglomerating the two $n=0$ and two $n=1$ states in writing ξ as a sum over $n\in\{0,1\}$.

Type	Description	Symbol
material parameter	potential energy of gas molecule adsorbed on site ♡	$\epsilon_{\heartsuit}$
material parameter	potential energy of gas molecule adsorbed on site △	$\epsilon_{\triangle}$
material parameter	energetic penalty for the wheel to occupy △ station	δ
microstate variable	number of adsorbed gas molecules in the RMS-MOF unit cell	n
microstate variable	position of the wheel ($r = 0 \implies \heartsuit$, $r = 1 \implies \triangle$)	r
macrostate variable	chemical potential set by bulk gas phase	μ
macrostate variable	thermodynamic beta $1/(k_{\mathrm{B}}T)$ set by bulk gas phase	β

Table 3: Description of model parameters/variables

3.1.1 The gas adsorption isotherm

The expected number of adsorbed gas molecules in the RMS-MOF (i.e., the adsorption isotherm) is:

$$\langle n \rangle(P,T) = \left(\frac{\partial \log \xi}{\partial(\beta\mu)} \right)_{\beta} = \frac{K}{1 + K\beta P} \beta P, \tag{46}$$

where K depends on the Helmholtz free energy difference between the fixed $n = 1$ and $n = 0$ coarse-grained states in Sec. **??**:

$$K(T) \equiv \frac{q_{n=1}(T)}{q_{n=0}(T)} = e^{-\beta[A_{n=1}(T) - A_{n=0}(T)]}, \tag{47}$$

and describes the effective affinity of the gas for the RMS-MOF. To see how K depends on temperature and the interaction of the wheel and gas with the stations/sites on the RMS-MOF, we write K more explicitly:

$$K(T) = \frac{1}{1 + e^{-\beta\delta}} e^{-\beta\epsilon_{\triangle}} + \frac{e^{-\beta\delta}}{1 + e^{-\beta\delta}} e^{-\beta\epsilon_{\heartsuit}}. \tag{48}$$

To arrive at eqn. 46, we substituted $e^{\beta\mu}$ with βP by treating the bulk gas phase as an ideal [lattice] gas (see Sec. 2.3). We wrote $\langle n \rangle = (\cdots)\beta P$ to readily compare the density of gas in the RMS-MOF with that of the ideal [lattice] gas, βP. At low coverage, $\langle n \rangle \approx K\beta P$, and thus $K\beta$ is the Henry coefficient of gas in the RMS-MOF. If the RMS-MOF does not offer an energetic incentive for a gas molecule to adsorb from the gas phase, the density of gas in the RMS-MOF at low coverage is equal to the bulk ideal [lattice] gas ($\epsilon_{\triangle} = \epsilon_{\heartsuit} = 0 \implies K = 1$); as $\epsilon_{\triangle}$ and $\epsilon_{\heartsuit}$ decrease from zero, the gas in the RMS-MOF densifies.

Fig. 3 displays the adsorption isotherm of the RMS-MOF, which exhibits a functional form/shape equivalent to that of a single-site Langmuir model. However, we refer to K in eqn. 48 as the "pseudo"-Langmuir constant of the RMS-MOF because its relationship with temperature is more complicated than in an ordinary, single-site Langmuir model. In a Langmuir model offering a single adsorption site □ with gas-□ interaction energy $\epsilon_{\square}$, the Langmuir constant is $K_L(T) = e^{-\beta\epsilon_{\square}}$ (see Sec. 2.4); compare to eqn. 48. Satisfying our intuition, the pseudo-Langmuir constant K in eqn. 48 of the RMS-MOF is a weighted average of the Langmuir constants of a single-△-site and a single-♡-site Langmuir model; the weights are determined by the probability that the wheel occupies the ♡ and △, respectively, in the $n = 0$ Canonical ensemble. Trivially, the RMS-MOF is equivalent to a single-△-site and single-♡-site Langmuir model in the limit $\delta \to \infty$ and

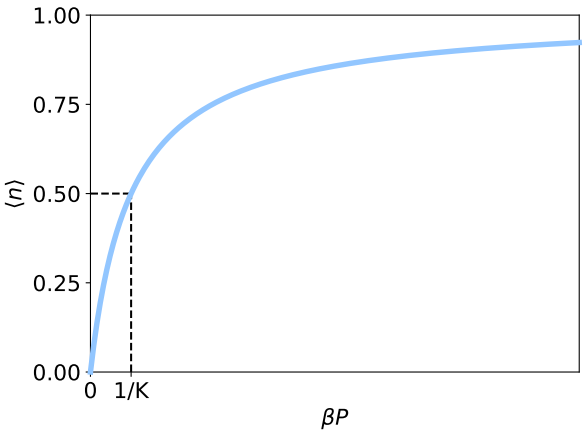

Figure 3: The adsorption isotherm of our model RMS-MOF, given by eqn. 46, exhibits an identical shape as that of a single-site Langmuir model. The pseudo-Langmuir constant K of the RMS-MOF, given in eqn. 48, describes its effective affinity for gas; when immersed in an ideal gas with density $1/K$, half of the adsorption sites in the RMS-MOF are occupied by a gas molecule.

$\delta \to -\infty$, respectively, as the wheel is then fixed on a single station and, invariably, only one adsorption site is exposed to the gas. Less trivially, the RMS-MOF is equivalent to a (i) single-♡-site Langmuir model when the gas has no preference for a station ($\epsilon_\heartsuit = \epsilon_\triangle$), since then the position of the wheel is inconsequential to energy of interaction of the gas with the RMS-MOF and (ii) single-site Langmuir model with gas-site interaction energy ($\epsilon_\heartsuit + \delta$) when $\epsilon_\triangle = \epsilon_\heartsuit + 2\delta$. In both cases (i) and (ii), we find that the functional form of $K(T)$ in eqn. 48 is equivalent to that of $K_L(T)$. Other than these cases, we will see that the RMS-MOF model differs non-trivially from a single-site Langmuir model owing to the entropy arising from the wheel.

3.1.2 The position of the wheel

The expected value of r, the probability that the wheel occupies the △ station, is:

$$\langle r \rangle(P,T) = -\left(\frac{\partial \log \xi}{\partial(\beta\delta)}\right)_\beta \tag{49}$$

$$= \left(\frac{e^{-\beta\delta}}{1+e^{-\beta\delta}}\right)\left(\frac{1+e^{-\beta\epsilon_\heartsuit}\beta P}{1+K\beta P}\right) \tag{50}$$

where K is the temperature- and material-dependent psuedo-Langmuir constant given in eqn. 48. As $P \to 0^+$, the RMS-MOF empties of gas and $\langle r \rangle(P,T) \to \langle r \rangle_{n=0}(T)$. As P increases from zero and gas fills the RMS-MOF, there are three possibilities. If △ is the more favorable adsorption site for the gas ($\epsilon_\triangle < \epsilon_\heartsuit \implies K > e^{-\beta\epsilon_\heartsuit}$), $\langle r \rangle$ decreases with pressure (and gas adsorption); i.e., more of the wheels occupy the ♡ station as gas fills the RMS-MOF. If the ♡ station is the more favorable gas adsorption site, more of the wheels occupy the △ station as gas fills the RMS-MOF. Fig. 4 illustrates these two cases. Both outcomes are understood from the viewpoint of the gas *competing* with the wheel for its favorite adsorption site. The third case where gas has no preference for a station lacks such competition, and adsorbed gas does not affect the position of the wheel: $\epsilon_\heartsuit = \epsilon_\triangle \implies K = e^{-\beta\epsilon_\heartsuit}$, then eqn. 50 recovers $\langle r \rangle$ is independent of P. In the limit $P \to \infty$, each

adsorption site is occupied by gas (via eqn. 46) and $\langle r\rangle(P,T) \to \langle r\rangle_{n=1}(T)$. This is seen by using eqn. 46 to rewrite eqn. 50 and directly relate the wheel in the RMS-MOF gas system in the grand-canonical ensemble to the two coarse-grained models in Sec. **??**:

$$\langle r\rangle = (1 - \langle n\rangle)\,\langle r\rangle_{n=0} + \langle n\rangle\langle r\rangle_{n=1} \tag{51}$$

This form reveals that the wheel transitions from the fixed $n = 0$ two-state model to the fixed $n = 1$ state model as gas fills the RMS-MOF.

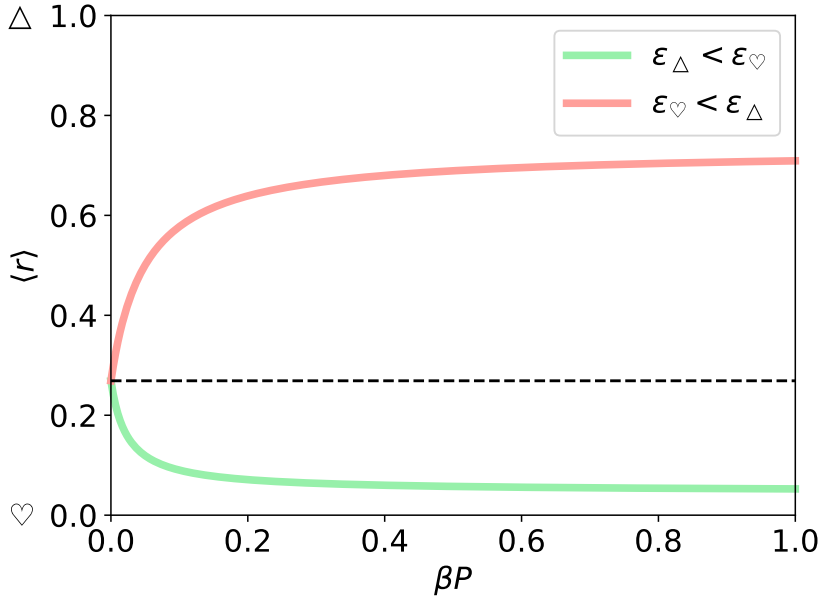

Figure 4: The probability that the wheel in the RMS-MOF occupies the △ station as a function of the density of the ideal gas in which the RMS-MOF is immersed. $\langle r\rangle$ is shown at fixed β for two RMS-MOFs, both with $\beta\delta = 1$. The horizontal dashed line shows $\langle r\rangle_{n=0}$ for both RMS-MOFs when empty of gas. In one RMS-MOF, ♡ is a more favorable gas adsorption site than △ ($\beta\epsilon_{\heartsuit} = -4, \beta\epsilon_{\triangle} = -2$), and the wheel is increasingly likely to occupy the △ station as gas adsorbs. In the other RMS-MOF, △ is a more favorable gas adsorption site than ♡ ($\beta\epsilon_{\triangle} = -4, \beta\epsilon_{\heartsuit} = -2$), and the wheel is increasingly likely to occupy the ♡ station as gas adsorbs. These (different) outcomes are caused by competition between the wheel and gas for the station/adsorption site and demonstrate the degree of control that we have over the RMS-MOf's behavior by tuning only two parameters.

The perspective of the wheel as a transition between two two-state models as gas fills the RMS-MOF uncovers interesting temperature-dependence of $\langle r\rangle$. In the empty RMS-MOF, the minimum-energy state for the wheel is the ♡ station ($\delta > 0$). When the RMS-MOF is full of gas: if $\epsilon_{\triangle} < \delta + \epsilon_{\heartsuit}$, the minimum-energy state is still the one where the wheel sits at the ♡ station; if $\epsilon_{\heartsuit} + \delta < \epsilon_{\triangle}$, however, the minimum-energy state is the one where the wheel sits at the △ station. Interestingly, in the latter case illustrated in Fig. 5a, the station that the wheel occupies in the minimum-energy state of the RMS-MOF-gas system must then *switch*

at some gas pressure. As a consequence, because an increase in temperature induces the system to visit higher energy states more frequently, temperature increases affect the wheel differently depending on the amount of gas adsorbed if $\epsilon_{\heartsuit} + \delta < \epsilon_{\triangle}$. Fig. 5b shows the temperature-dependence of $\langle r \rangle$ at a sequence of fixed pressures for a RMS-MOF such that $\epsilon_{\heartsuit} + \delta < \epsilon_{\triangle}$. In this RMS-MOF empty of gas ($P = 0$), an increase in temperature induces the wheel to occupy the $\triangle$ station more frequently since this is the higher-energy state (see blue curve, $\langle r \rangle_{n=0}(\beta)$). In this RMS-MOF full of gas ($P \to \infty$), an increase in temperature induces the wheel to occupy the $\heartsuit$ station more frequently since this is the higher-energy state (see yellow curve, $\langle r \rangle_{n=1}(\beta)$). As β increases and gas fills the RMS-MOF at fixed (nonzero and finite) pressure, Fig. 5b illustrates the transition of the wheel from the decreasing function $\langle r \rangle_{n=0}(\beta)$ to the increasing function $\langle r \rangle_{n=1}(\beta)$ as it fills with gas; consequently, $\langle r \rangle(T; P)$ is non-monotonic in RMS-MOFs such that $\epsilon_{\heartsuit} + \delta < \epsilon_{\triangle}$. While we cannot speculate on a practical application, this non-monotonic temperature dependence of $\langle r \rangle(T; P)$ is interesting and unexpected.

3.1.3 The energy change upon gas adsorption

The expected energy of the RMS-MOF-gas system is:

$$\langle U \rangle = (1 - \langle n \rangle) \langle U \rangle_{n=0} + \langle n \rangle \langle U \rangle_{n=1}. \tag{52}$$

Analogous to $\langle r \rangle(P, T)$ in eqn. 51, $\langle U \rangle(P, T)$ is an interpolation between $\langle U \rangle_{n=0}(T)$ and $\langle U \rangle_{n=1}(T)$ in the fixed $n = 0$ and $n = 1$ two-state models using $\langle n \rangle(P, T)$ as a weight.

The differential energy of adsorption is the change in energy of the [macroscopic] RMS-MOF system when a molecule adsorbs from the gas phase at constant temperature and is of practical importance because it determines the heat released upon adsorption (at fixed pressure) and thus temperature-raises/drops in the adsorbent upon ad/de-sorption. [57]. For our model RMS-MOF, via eqn. 52, the differential energy of adsorption is:

$$\left(\frac{\partial \langle U \rangle}{\partial \langle n \rangle} \right)_{\beta} = \langle U \rangle_{n=1} - \langle U \rangle_{n=0}. \tag{53}$$

Intuitively, the differential energy of adsorption is the difference between the average energy in the fixed $n = 1$ state model and the fixed $n = 0$ state model.

Notably, the differential energy of adsorption in eqn. 53 is not a function of $\langle n \rangle$ because the adsorption of a gas molecule i in our model RMS-MOF crystal cannot influence the free energy of adsorption of the next gas molecule $i + 1$ that adsorbs. In contrast, the differential energy of adsorption is a function of $\langle n \rangle$ if adsorbed gas (i) induces a change in the structure of the material that affects the interaction with the next adsorbate, (ii) provides gas-gas attractions for further adsorbed gas molecules, or (iii) occupies and excludes other adsorbates from lower energy adsorption sites and forces further adsorbed molecules to occupy higher energy sites. For an example of case (ii), see Ref. [54] where gas adsorbs and induces a ligand that is shared between two unit cells to rotate, thereby changing the interaction energy of the gas with the material in a neighboring unit cell.

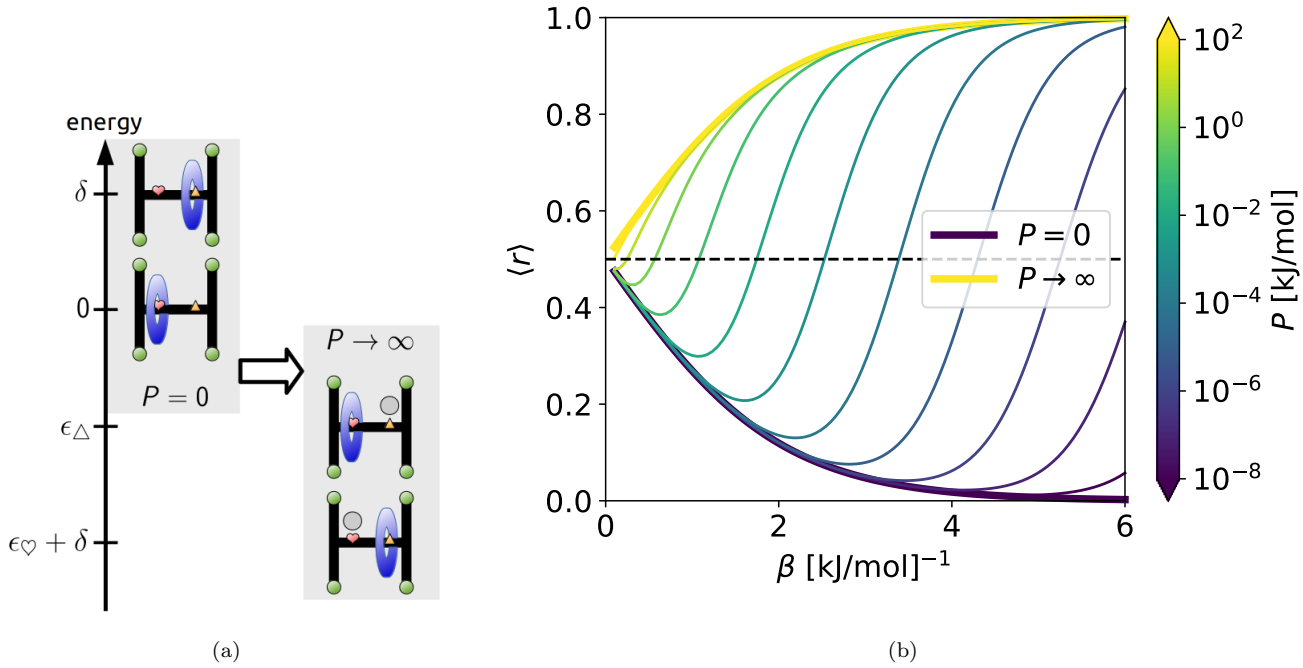

(a) (b)

Figure 5: Owing to gas-wheel competition for the ♡ site/station, the position of the wheel in an RMS-MOF such that $\epsilon_\heartsuit + \delta < \epsilon_\triangle$ responds to temperature changes differently depending on the amount of gas adsorbed. (a) Starting from empty, the RMS-MOF-gas system transitions from a $(0, \delta)$ two-state model to a $(\epsilon_\triangle, \epsilon_\heartsuit + \delta)$ two-state model as it fills with gas. If $\epsilon_\heartsuit + \delta < \epsilon_\triangle$, the wheel sits at opposite stations in the minimum energy states of the system corresponding to $P = 0$ and $P \to \infty$. Thus, increases in temperature affect each fixed $n \in \{0, 1\}$ state oppositely. (b) The two thicker curves show $\langle r \rangle_{n=0}$ and $\langle r \rangle_{n=1}$ for the RMS-MOF empty (bottom) and full (top) of gas, both corresponding to the two two-state models in (a). Starting from the high temperature limit (horizontal line, $\langle r \rangle \to 0.5$), decreasing the temperature at fixed pressure causes $\langle r \rangle$ to decrease until a certain point, then it increases. This non-monotonicitiy can be explained as a transition between the two two-state models in (a) as gas fills the RMS-MOF as it is cooled (see eqn. 51). Here, $\delta = 1$, $\epsilon_\triangle = -1$, $\epsilon_\heartsuit = -3$ kJ/mol. Note that $\beta \propto \frac{1}{T}$

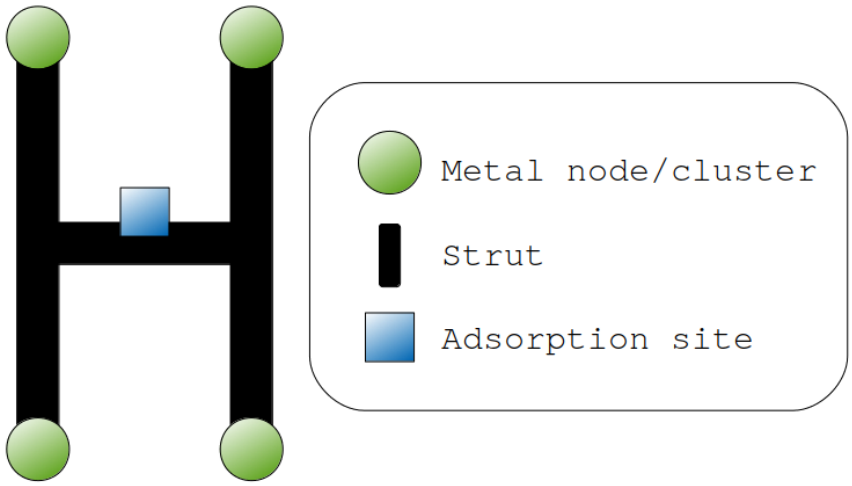

(a)

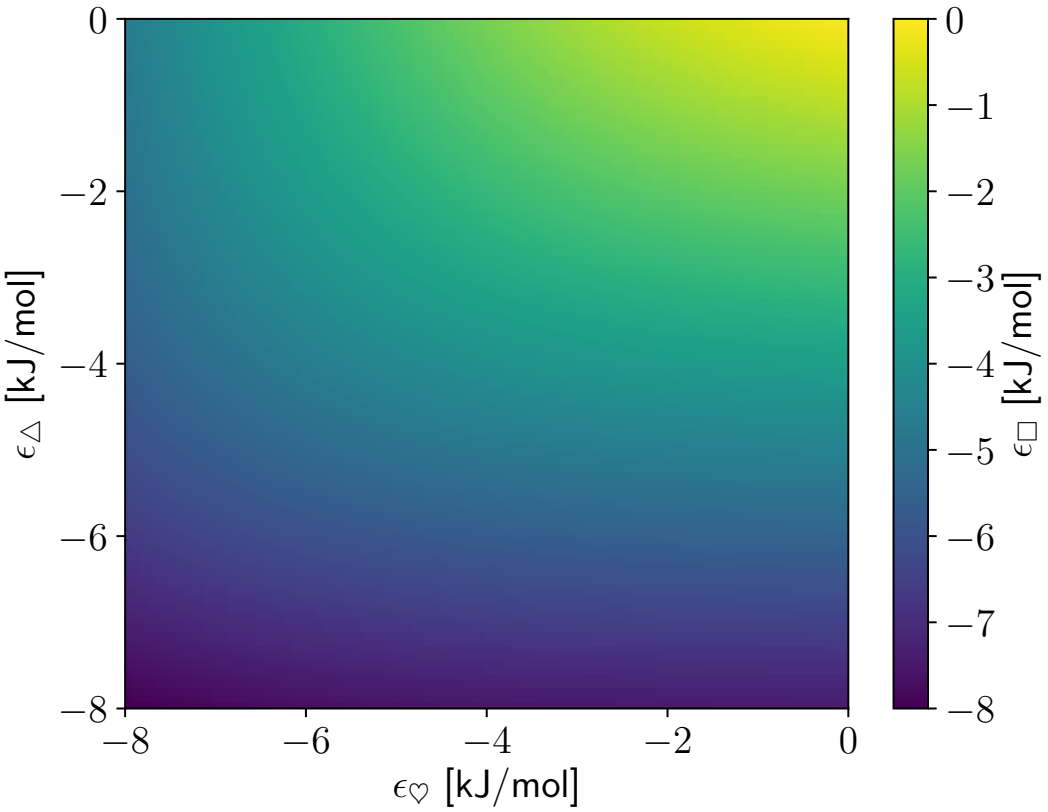

(b)

Figure 6: A single-□-site Langmuir model and its gas-□ interaction energy required to yield an identical adsorption isotherm as the RMS-MOF at room temperature T_0. (a) The unit cell of a single-□-site Langmuir model offers a single adsorption site □ with gas-box interaction energy $\epsilon_\square$. (b) Color shows $\epsilon_\square$ in the Langmuir model such that its adsorption isotherm at T_0 is equivalent to that of the RMS-MOF. The plane shows a slice of material space ($\delta = 3$ kJ/mol fixed).

3.2 Comparison to a single-site Langmuir model

The gas adsorption isotherm of the RMS-MOF in eqn. 46 and Fig. 3 exhibits an identical functional form/shape as a single-site Langmuir adsorption isotherm, yet the pseudo-Langmuir constant K in eqn. 48 is a more complicated function of temperature than the Langmuir constant of an ordinary Langmuir model, $K_L = e^{-\beta\epsilon_\square}$. As suggested by the latter finding, we next explore how the adsorption properties of the RMS-MOF fundamentally differ from a Langmuir model that exhibits the same gas adsorption isotherm as the RMS-MOF at a given temperature. In particular, we show that, depending on the interactions of the wheel and gas with the stations/sites, (i) adsorption is more or less sensitive to changes in temperature and (ii) more or less heat is released upon adsorption.

For the comparisons of the RMS-MOF to a single-$\square$-site Langmuir model below, we assign the energy of the gas-$\square$ interaction $\epsilon_\square$ such that the Langmuir material and RMS-MOF exhibit identical adsorption isotherms at room temperature, T_0. Figure 6 shows the $\epsilon_\square$ that equates the Langmuir and psuedo-Langmuir constants, $K_L(T_0) = K(T_0)$, and thus equates the adsorption isotherms at T_0 in the Langmuir material and RMS-MOF. Sec. 2.4 provides a detailed derivation of the adsorption isotherm of the Langmuir model, which is also obtained in eqn. 48 via setting $\delta = 0$ and $\epsilon_\square \equiv \epsilon_\heartsuit = \epsilon_\triangle$.

3.2.1 Temperature-sensitivity of adsorption

Porous materials that exhibit either temperature-sensitive or temperature-insensitive adsorption are useful for engineering applications. Temperature-sensitive gas adsorption facilitates temperature-swing adsorption processes for gas storage and separations, where temperature increases are used to regenerate the adsorbent and expel its adsorbed gas. Temperature-insensitive gas adsorption minimizes pressure variations in adsorbed gas storage vessels exposed to a large range of temperatures. Gas sensors based on gravimetric adsorption in porous materials also benefit from temperature-insensitive adsorption when operating in a large range of temperatures.

We now investigate how the temperature-dependence of adsorption in an RMS-MOF differs from a single-$\square$-site Langmuir model with an identical adsorption isotherm at temperature T_0. i.e., we determine whether more or less gas will be desorbed from the RMS-MOF than from the Langmuir model upon a differential increase in temperature at fixed pressure.

Fig. 7a compares the temperature-sensitivity of the Henry coefficients of RMS-MOF and Langmuir model by using color to depict $\frac{\partial(K\beta)}{\partial T}|_{T_0} / \frac{\partial(K_L\beta)}{\partial T}|_{T_0}$ as a function of the gas-$\heartsuit$ and gas-$\triangle$ interaction energies (fixed δ). We show in Sec. 2.5 that this ratio of the temperature-sensitivities of the Henry coefficients is equal to the ratio of the temperature-sensitivities of adsorption at any pressure. Unsurprisingly, adsorption is equally temperature-sensitive in the RMS-MOFs and Langmuir materials along the planes in material space $\epsilon_\heartsuit = \epsilon_\triangle$ or $\epsilon_\triangle = \epsilon_\heartsuit + 2\delta$ (the dashed lines in Fig. 7a), since then the RMS-MOF is equivalent to the Langmuir model. For RMS-MOFs falling in the pink region, $\langle n \rangle$ is less sensitive to temperature changes than in the Langmuir materials, where as the green region $\langle n \rangle$ is more sensitive. To illustrate, isobars in the less- and more-temperature sensitive RMS-MOFs marked in Fig. 7a are shown in Figs. 7b and 7c along with isobars

of the Langmuir model for comparison.

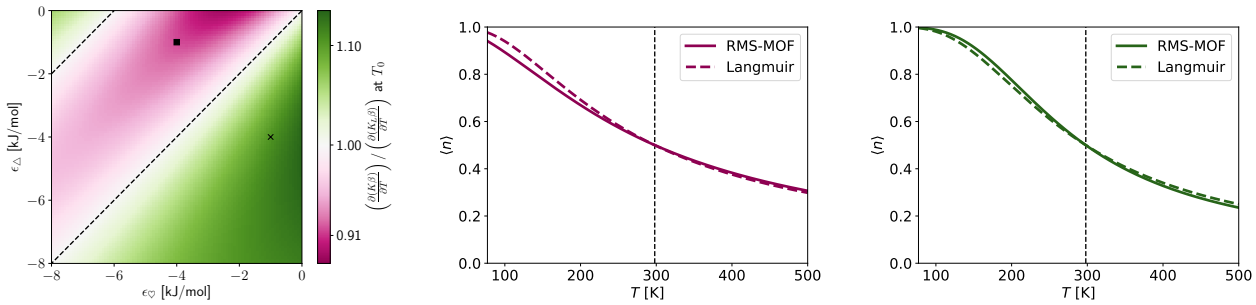

(a) (b) (c)

Figure 7: Depending on the interaction of the wheel and gas with the stations/sites, adsorption in the RMS-MOF can be more less or more sensitive to temperature changes than in a single-site Langmuir material with an identical adsorption isotherm at room temperature T_0. (a) The plane is a slice of RMS-MOF material space ($\delta = 3$ kJ/mol fixed). Color depicts the ratio of the temperature-sensitivity of the Henry coefficient of a RMS-MOF, $K\beta$, to that of the Langmuir material, $K_L\beta$. RMS-MOFs in the pink and green region exhibit less and more temperature-sensitive adsorption than the Langmuir materials respectively. Dashed lines correspond to $\epsilon_\heartsuit = \epsilon_\triangle$ and $\epsilon_\heartsuit + 2\delta = \epsilon_\triangle$. (b, c) Isobars ($P$ set to achieve $\langle n\rangle = 0.5$ at temperature T_0) for the two RMS-MOFs represented as a square (b) and x (c) in (a). Vertical line denotes T_0.

The difference in temperature-sensitivity of adsorption between the RMS-MOF and single-site Langmuir material is owed to the entropy imparted by the wheel. The analogy of eqn. 47 holds for the Langmuir material as well (see eqn. 27); thus, if a single-site Langmuir material and RMS-MOF possess identical adsorption isotherms, they must possess equal free energy changes upon adsorption at that temperature. Via (i) temperature-differentiation of the Henry coefficient $K\beta$ using the form in eqn. 47 and (ii) the analogy of eqn. 47 for the Langmuir material (see eqn. 27):

$$K(T_0) = K_L(T_0) \implies \frac{\partial(K\beta)}{\partial T} - \frac{\partial(K_L\beta)}{\partial T} = \frac{K}{(k_\mathrm{B}T)^2}(S_{n=1} - S_{n=0}) \text{ at } T_0. \tag{54}$$

See Sec. 2.5 for an expanded derivation. According to eqn. 54, the difference in Henry coefficient temperature-sensitivities is related to the difference in entropy of the two coarse-grained states of the RMS-MOF given in eqns. 5 and 9. The cause of the difference in temperature-sensitivity of adsorption between the RMS-MOF and Langmuir material thus lies in how the adsorption of gas changes the entropy of the wheel in the RMS-MOF. If the addition of a gas molecule to the RMS-MOF unit cell increases the entropy of the wheel, gas adsorption is less temperature-sensitive in the RMS-MOF than in the Langmuir material with the same adsorption isotherm at temperature T_0. The inverse also hold, a decrease in entropy with the addition of gas will lead to a more temperature sensitive gas adsorption.

The region of RMS-MOF material space where the adsorption of gas increases the entropy of the RMS-MOF is (see Sec. 2.5.5):

$$S_{n=1} > S_{n=0} \iff \epsilon_\heartsuit < \epsilon_\triangle < \epsilon_\heartsuit + 2\delta, \tag{55}$$

the pink band in Fig. 7a. In words, $S_{n=1} > S_{n=0}$ iff both (i) the interaction of the gas with the $\heartsuit$ site is more favorable than with the $\triangle$ site ($\epsilon_\heartsuit < \epsilon_\triangle$) and (ii) the preference of the gas for the $\heartsuit$ site over the $\triangle$ site is limited to 2δ ($\epsilon_\triangle < \epsilon_\heartsuit + 2\delta$). Because $\delta > 0$, condition (i) ensures that gas adsorption causes the wheel to occupy the $\triangle$ station more often (see Fig. 4), as gas will compete with and thus to an extent exclude the wheel for/from the $\heartsuit$ station; this increases the entropy of the RMS-MOF-gas system provided that condition (ii) also holds. If condition (i) held but condition (ii) did not, the gas would exclude the wheel from the $\heartsuit$ station more than the penalty $\delta > 0$ excluded the wheel from the $\triangle$ station when the gas was absent, thereby reducing the entropy from $S_{n=0}$.

3.2.2 Heat released upon adsorption

Porous materials that release much or little heat upon adsorption are useful for engineering applications. For gas storage and separations, porous materials that release minimal heat upon adsorption mitigate raises in temperature of the adsorbent bed upon gas charging that detriment its adsorptive uptake [11]. In contrast, porous materials that release a lot of heat upon adsorption are desired for thermal energy storage [34].

The enthalpy of adsorption in the RMS-MOF, which determines the heat released upon gas adsorption (at constant pressure), is the differential energy of adsorption given in eqn. 53 minus $k_\mathrm{B}T$ to account for PV work (via ideal gas law) [57].

We now investigate how the differential energy of adsorption in an RMS-MOF differs from a single-□-site Langmuir model with an identical adsorption isotherm at temperature T_0. For comparison, the differential energy of adsorption for a single-□-site Langmuir model is $\left(\frac{\partial\langle U_L\rangle}{\partial\langle n_L\rangle}\right)_\beta = \epsilon_\square$ (see Sec. 2.4).

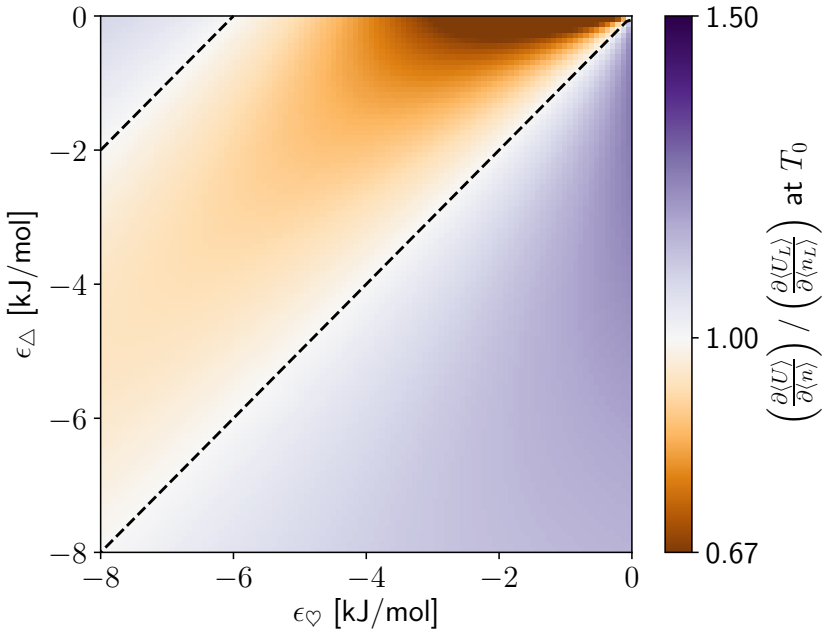

Figure 8: Depending on the interaction of the wheel and gas with the station/site, the differential energy of adsorption in the RMS-MOF can be more or less than in the Langmuir material with an identical adsorption isotherm at room temperature T_0. The plane is a slice of RMS-MOF material space ($\delta = 3$ kJ/mol fixed). Color depicts the ratio of the differential energy of adsorption of the RMS-MOF in eqn. 53 to that of the Langmuir material, $\epsilon_\square$. In the orange region, less heat is released upon adsorption in the RMS-MOF than in the Langmuir material. While in the n the purple region, more heat is released upon adsorption in the RMS-MOF than in the Langmuir material. Dashed lines correspond to $\epsilon_\heartsuit = \epsilon_\triangle$ and $\epsilon_\heartsuit + 2\delta = \epsilon_\triangle$.

Fig. 8 uses color to depict the ratio of the differential energy of adsorption in the RMS-MOF in eqn. 53 to that of the Langmuir material, $\epsilon_\square$, with the same adsorption isotherm at room temperature. RMS-MOFs falling in the orange region release less heat upon adsorption than the Langmuir material and those falling in the orange region will release more. Unsurprisingly, the ratio is unity on the planes within material space, $\epsilon_\heartsuit = \epsilon_\triangle$ and $\epsilon_\triangle = \epsilon_\heartsuit + 2\delta$ (dashed black lines), since then the RMS-MOF is equivalent to a Langmuir model.

The difference in differential energy of adsorption in Fig. 8 again owes to the entropy of the wheel in the RMS-MOF. Rewrite eqn. 53 in terms of free energy $A \equiv \langle U\rangle - TS$:

$$\left(\frac{\partial\langle U\rangle}{\partial\langle n\rangle}\right)_\beta = A_{n=1} - A_{n=0} + T(S_{n=1} - S_{n=0}) \tag{56}$$

Applying eqn. 47, the difference in the differential energies of adsorption is determined by the change in entropy of the wheel upon the addition of a gas molecule to the RMS-MOF unit cell:

$$K(T_0) = K_L(T_0) \implies \left(\frac{\partial\langle U\rangle}{\partial\langle n\rangle}\right)_\beta - \left(\frac{\partial\langle U_L\rangle}{\partial\langle n\rangle}\right)_\beta = T\left(S_{n=1} - S_{n=0}\right) \text{ at } T_0. \tag{57}$$

If $S_{n=1} > S_{n=0}$, the RMS-MOF releases less heat upon adsorption than the Langmuir model. Thus, via eqn. 55, RMS-MOFs falling in the region of material space $\epsilon_\heartsuit < \epsilon_\triangle < \epsilon_\heartsuit + 2\delta$ (orange band in Fig. 8) exhibit less heat upon adsorption than the Langmuir material with the same adsorption isotherm.

The entropy change upon adsorption, $S_{n=1} - S_{n=0}$, is implicated in both how the temperature-sensitivity of the Henry coefficients and the heat released upon adsorption differ from a Langmuir model with the same adsorption isotherm via eqns. 54 and 57, respectively. Equation 44 confirms that the temperature-sensitivity of adsorption is intimately connected to the energy change upon adsorption, which explains the resemblance between Figs. 7a and 8 and the same conditions for when the ratios are unity.

3.2.3 Summary

In summary, if $\epsilon_\heartsuit < \epsilon_\triangle < \epsilon_\heartsuit + 2\delta$, compared to a Langmuir material with an identical adsorption isotherm at temperature T_0, the RMS-MOF (i) exhibits less temperature-sensitive adsorption and (ii) releases less heat upon adsorption. This is caused by an increase in the entropy of the wheel upon the addition of a gas molecule. Note in Fig. 7a an apparent symmetry about $\epsilon_\triangle = \epsilon_\heartsuit + \delta$; along this plane in material space, the entropy of the fixed $n = 1$ state, $S_{n=1}$ in eqn. 9, is maximized because the energies of the two possible microstates are equal. This symmetry is also present in eqn. 57 but is obscured in Fig. 8 because we inspect the ratio instead of the difference.

The difference in temperature-sensitivity of adsorption between the RMS-MOF and Langmuir material in Fig. 7b is not dramatic. Because there are only two microstates that correspond to fixed $n \in \{0, 1\}$, $|S_{n=1} - S_{n=0}| \leq \log 2$, limiting the difference in both the temperature-sensitivity of adsorption (normalized by K) in eqn. 54 and differential energy of adsorption in eqn. 57 between the Langmuir and RMS-MOF model materials. However, this entropic effect may be more dramatic when fully accounting for the degrees of freedom of a wheel in an RMS-MOF, such as translation along a continuum of states on the strut, circumrotation, and motion orthogonal to the axle.

4 Discussion of results and directions for future research

4.1 Discussion of results

Since 1918, when Langmuir introduced the single-site adsorption model [56], many molecular-level adsorption models have been developed [56, 30] to explain and predict adsorption phenomena from the bottom-up. The modular and adjustable nature of MOFs has expanded the scope of complexity we can integrate into porous materials, e.g. dynamic structures that *respond* to gas adsorption [31, 48, 16, 12, 38] and, consequently, exhibit unique adsorption properties [17]. We may be seeing a renaissance of simple, molecular-level statistical mechanical adsorption models to explain and predict exotic adsorption properties in these dynamic, gas-responsive materials, as exemplified by models to explain inflections in adsorption isotherms caused by gas-induced ligand rotation [54], negative gas adsorption [42, 23], discontinuities in adsorption isotherms [19], gas-induced framework expansion/contraction [20, 28, 58], sharp steps in CO_2 adsorption via the formation of ammonium carbamate chains [37], etc.

In this work, we developed a statistical mechanical model of gas adsorption in a metal-organic framework harboring a rotaxane molecular shuttle in its pores, an RMS-MOF. We formulated a very simple abstraction of an RMS-MOF similar in spirit to the seminal Langmuir adsorption model, with the aim to explore whether unique or enhanced adsorption properties could be imparted to a MOF by a shuttling wheel. Our simple model of a RMS-MOF provides useful insights into how gas adsorption is affected by (i) the competition between the wheel and gas for adsorption sites on the MOF strut and (ii) the thermal motion of the wheel. We explained how gas adsorption, the state of the wheel, and the energy change upon adsorption depend on temperature, pressure, and the interaction of the wheel and gas with the stations/sites. While we found the gas adsorption isotherm to exhibit an identical shape as a single-site Langmuir model, the dependence of the psuedo-Langmuir constant of the RMS-MOF on temperature fundamentally differs from a Langmuir model. As hinted by the latter observation, we found two ways that adsorption in the RMS-MOF fundamentally differs from a Langmuir material, owing to the entropy of the shuttling wheel. Depending on the interaction of the wheel and gas for the stations/sites, compared to a Langmuir material with an identical adsorption isotherm at temperature T_0, (i) adsorption can more or less temperature-sensitive and (ii) more or less heat can be released upon adsorption. Both properties are useful for engineering applications and emanate from the entropy of the shuttling wheel in the RMS-MOF. Finally, we found that if the gas out-competes the wheel for its favorite station, temperature changes affect the position of the wheel non-monotonically.

Regarding the pursuit of RMS-MOFs for storing and separating gases, we have an "elephant in the room": the elephant is the macrocycle wheel wrapped around the strut of the MOF scaffold, and the room is the pore space in the MOF. This large macrocycle wheel occupies precious porosity that could otherwise host another gas molecule; the wheel imposes the limitation that fewer adsorption sites for gas molecules can be packed into a fixed volume of MOF. Therefore, the necessarily reduced porosity of a RMS-MOF as well as its synthetic complexity must be compensated for by its enhanced adsorption properties to see application in gas storage and separations.

4.2 directions for future research

Future work remains to chart further exotic adsorption properties offered by metal-organic frameworks harboring rotaxane molecular shuttles. To confirm our predictions herein, heroic experimental efforts are needed to synthesize a porous, activated RMS-MOF, measure its gas adsorption properties, and characterize *in situ* the internal state of its macrocycle wheel as a function of gas adsorption. Thus far, only one MOF harboring a rotaxane shuttle has been synthesized [65]. Some remaining knowledge gaps could be filled by extending our model. First, our toy model could be decorated with complexity to account for other molecular features that can be engineered into RMS-MOFs: (i) a radially asymmetric macrocycle on the rotaxane, whose rotational conformations expose different functional groups to the stations (see Ref. [4]), (ii) multiple stations [and, thus, adsorption sites] on the axle of the rotaxane, (iii) multiple macrocycle wheels threaded around the axle of the rotaxane [24], and (iv) arranging molecular shuttles in a MOF in a more complicated topology to allow coupling between neighboring molecular shuttles (inspired by Ref. [47]) and (v) allowing multiple gas molecules to adsorb in a unit cell. Outside the context of MOFs, Sevick and Williams developed and analyzed a statistical mechanical model of radially asymmetric wheels [52] [case (i)] and multiple wheels [50, 51, 53] [case (iii)] in a rotaxane molecular shuttle and uncovered interesting behavior. Second, analyzing our model RMS-MOF immersed in a mixture of gases could reveal enhanced selectivity arising from the molecular shuttle. Intriguingly, gas adsorption in the RMS-MOF in Fig. 1 bears some resemblance to biomolecular recognition where e.g. a ligand binds to a protein and induces a shift in its conformational ensemble [7]. Third, modeling can shed light on the interplay of external stimuli and adsorption in MOFs with stimuli-responsive rotaxanes [62] integrated into them. Fourth, atomistic models of RMS-MOFs could explore the practical constraints on material space (δ, $\epsilon_{\heartsuit}$, $\epsilon_{\triangle}$) and suggest explicit RMS-MOF chemistry to pursue for anomalous adsorption properties.

References

[1] J. M. Abendroth, O. S. Bushuyev, P. S. Weiss, and C. J. Barrett. Controlling motion at the nanoscale: rise of the molecular machines. *ACS Nano*, 9(8):7746–7768, 2015.

[2] M. D. Allendorf, R. J. Houk, L. Andruszkiewicz, A. A. Talin, J. Pikarsky, A. Choudhury, K. A. Gall, and P. J. Hesketh. Stress-induced chemical detection using flexible metal- organic frameworks. *Journal of the American Chemical Society*, 130(44):14404–14405, 2008.

[3] P. L. Anelli, N. Spencer, and J. F. Stoddart. A molecular shuttle. *Journal of the American Chemical Society*, 113(13):5131–5133, 1991.

[4] G. Baggi and S. J. Loeb. Rotationally active ligands: Dialing-up the co-conformations of a [2] rotaxane for metal ion binding. *Angewandte Chemie International Edition*, 55(40):12533–12537, 2016.

[5] V. Balzani, A. Credi, F. M. Raymo, and J. F. Stoddart. Artificial molecular machines. *Angewandte Chemie International Edition*, 39(19):3348–3391, 2000.

[6] B. R. Barnett, M. I. Gonzalez, and J. R. Long. Recent progress towards light hydrocarbon separations using metal–organic frameworks. *Trends in Chemistry*, 1(2), 2019.

[7] D. D. Boehr, R. Nussinov, and P. E. Wright. The role of dynamic conformational ensembles in biomolecular recognition. *Nature Chemical Biology*, 5(11):789, 2009.

[8] A. Boutin, M.-A. Springuel-Huet, A. Nossov, A. Gedeon, T. Loiseau, C. Volkringer, G. Férey, F.-X. Coudert, and A. H. Fuchs. Breathing transitions in mil-53 (al) metal–organic framework upon xenon adsorption. *Angewandte Chemie International Edition*, 48(44):8314–8317, 2009.

[9] C. J. Bruns and J. F. Stoddart. *The Nature of the Mechanical Bond: From Molecules to Machines*. John Wiley & Sons, 2016.

[10] K. Chang and O. Talu. Behavior and performance of adsorptive natural gas storage cylinders during discharge. *Applied Thermal Engineering*, 16(5):359 – 374, 1996.

[11] K. Chang and O. Talu. Behavior and performance of adsorptive natural gas storage cylinders during discharge. *Applied Thermal Engineering*, 16(5):359–374, 1996.

[12] Z. Chang, D.-H. Yang, J. Xu, T.-L. Hu, and X.-H. Bu. Flexible metal–organic frameworks: recent advances and potential applications. *Advanced Materials*, 27(36):5432–5441, 2015.

[13] H. J. Choi, M. Dinca, and J. R. Long. Broadly hysteretic h_2 adsorption in the microporous metal- organic framework co(1, 4-benzenedipyrazolate). *Journal of the American Chemical Society*, 130(25):7848–7850, 2008.

[14] A. Coskun, M. Banaszak, R. D. Astumian, J. F. Stoddart, and B. A. Grzybowski. Great expectations: can artificial molecular machines deliver on their promise? *Chemical Society Reviews*, 41(1):19–30, 2012.

[15] A. Coskun, M. Hmadeh, G. Barin, F. Gándara, Q. Li, E. Choi, N. L. Strutt, D. B. Cordes, A. M. Slawin, J. F. Stoddart, J.-P. Sauvage, and O. Yaghi. Metal–organic frameworks incorporating copper-complexed rotaxanes. *Angewandte Chemie International Edition*, 51(9):2160–2163, 2012.

[16] F.-X. Coudert. Responsive metal–organic frameworks and framework materials: under pressure, taking the heat, in the spotlight, with friends. *Chemistry of Materials*, 27(6):1905–1916, 2015.

[17] F.-X. Coudert and J. D. Evans. Nanoscale metamaterials: Meta-mofs and framework materials with anomalous behavior. *Coordination Chemistry Reviews*, 388:48–62, 2019.

[18] H. Deng, M. A. Olson, J. F. Stoddart, and O. M. Yaghi. Robust dynamics. *Nature Chemistry*, 2(6):439–443, 2010.

[19] L. J. Dunne and G. Manos. Exact matrix treatment of an osmotic ensemble model of adsorption and pressure induced structural transitions in metal organic frameworks. *Dalton Transactions*, 45(10):4213–4217, 2016.

[20] L. J. Dunne and G. Manos. Statistical mechanics of binary mixture adsorption in metal–organic frameworks in the osmotic ensemble. *Philosophical Transactions of the Royal Society A: Mathematical, Physical and Engineering Sciences*, 376(2115):20170151, 2018.

[21] S. K. Elsaidi, M. H. Mohamed, C. M. Simon, E. Braun, T. Pham, K. A. Forrest, W. Xu, D. Banerjee, B. Space, M. J. Zaworotko, and P. Thallapally. Effect of ring rotation upon gas adsorption in SIFSIX-3-M (M= Fe, Ni) pillared square grid networks. *Chemical Science*, 8(3):2373–2380, 2017.

[22] J. D. Evans, L. Bocquet, and F.-X. Coudert. Origins of negative gas adsorption. *Chem*, 1(6):873–886, 2016.

[23] J. D. Evans, S. Krause, S. Kaskel, M. B. Sweatman, and L. Sarkisov. Exploring the thermodynamic criteria for responsive adsorption processes. *Chemical Science*, 10(19):5011–5017, 2019.

[24] L. Fang, M. A. Olson, D. Benítez, E. Tkatchouk, W. A. Goddard III, and J. F. Stoddart. Mechanically bonded macromolecules. *Chemical Society Reviews*, 39(1):17–29, 2010.

[25] N. Farahani, K. Zhu, C. A. O'Keefe, R. W. Schurko, and S. J. Loeb. Thermally driven dynamics of a rotaxane wheel about an imidazolium axle inside a metal–organic framework. *ChemPlusChem*, 81(8):836–841, 2016.

[26] O. K. Farha, I. Eryazici, N. C. Jeong, B. G. Hauser, C. E. Wilmer, A. A. Sarjeant, R. Q. Snurr, S. T. Nguyen, A. Yazaydın, and J. T. Hupp. Metal–organic framework materials with ultrahigh surface areas: is the sky the limit? *Journal of the American Chemical Society*, 134(36):15016–15021, 2012.

[27] H. Furukawa, K. E. Cordova, M. O'Keeffe, and O. M. Yaghi. The chemistry and applications of metal-organic frameworks. *Science*, 341(6149):1230444, 2013.

[28] A. Ghysels, L. Vanduyfhuys, M. Vandichel, M. Waroquier, V. Van Speybroeck, and B. Smit. On the thermodynamics of framework breathing: A free energy model for gas adsorption in MIL-53. *The Journal of Physical Chemistry C*, 117(22):11540–11554, 2013.

[29] Y. He, W. Zhou, G. Qian, and B. Chen. Methane storage in metal–organic frameworks. *Chemical Society Reviews*, 43(16):5657–5678, 2014.

[30] T. L. Hill. *An introduction to statistical thermodynamics*. Courier Corporation, 1986.

[31] S. Horike, S. Shimomura, and S. Kitagawa. Soft porous crystals. *Nature Chemistry*, 1(9):695–704, 2009.

[32] R. Kitaura, K. Seki, G. Akiyama, and S. Kitagawa. Porous coordination-polymer crystals with gated channels specific for supercritical gases. *Angewandte Chemie International Edition*, 42(4):428–431, 2003.

[33] L. K. Knight, V. N. Vukotic, E. Viljoen, C. B. Caputo, and S. J. Loeb. Eliminating the need for independent counterions in the construction of metal–organic rotaxane frameworks (MORFs). *Chemical Communications*, (37):5585–5587, 2009.

[34] T. Kohler and K. Müller. Influence of different adsorbates on the efficiency of thermochemical energy storage. *Energy Science & Engineering*, 5(1):21–29, 2017.

[35] S. Krause, V. Bon, I. Senkovska, U. Stoeck, D. Wallacher, D. M. Többens, S. Zander, R. S. Pillai, G. Maurin, F.-X. Coudert, et al. A pressure-amplifying framework material with negative gas adsorption transitions. *Nature*, 532(7599):348, 2016.

[36] L. E. Kreno, K. Leong, O. K. Farha, M. Allendorf, R. P. Van Duyne, and J. T. Hupp. Metal–organic framework materials as chemical sensors. *Chemical Reviews*, 112(2):1105–1125, 2011.

[37] J. Kundu, J. F. Stilck, J.-H. Lee, J. B. Neaton, D. Prendergast, and S. Whitelam. Cooperative gas adsorption without a phase transition in metal-organic frameworks. *Physical Review Letters*, 121(1):015701, 2018.

[38] J. H. Lee, S. Jeoung, Y. G. Chung, and H. R. Moon. Elucidation of flexible metal-organic frameworks: Research progresses and recent developments. *Coordination Chemistry Reviews*, 389:161–188, 2019.

[39] J.-R. Li, R. J. Kuppler, and H.-C. Zhou. Selective gas adsorption and separation in metal–organic frameworks. *Chemical Society Reviews*, 38(5):1477–1504, 2009.

[40] S. J. Loeb. Metal–organic rotaxane frameworks; MORFs. *Chemical Communications*, (12):1511–1518, 2005.

[41] S. J. Loeb. Rotaxanes as ligands: from molecules to materials. *Chemical Society Reviews*, 36(2):226–235, 2007.

[42] G. Manos and L. Dunne. Predicting the features of methane adsorption in large pore metal-organic frameworks for energy storage. *Nanomaterials*, 8(10):818, 2018.

[43] J. A. Mason, J. Oktawiec, M. K. Taylor, M. R. Hudson, J. Rodriguez, J. E. Bachman, M. I. Gonzalez, A. Cervellino, A. Guagliardi, C. M. Brown, P. Llewellyn, N. Masciocchi, and J. Long. Methane storage in flexible metal–organic frameworks with intrinsic thermal management. *Nature*, 527(7578):357–361, 2015.

[44] P. Z. Moghadam, A. Li, S. B. Wiggin, A. Tao, A. G. Maloney, P. A. Wood, S. C. Ward, and D. Fairen-Jimenez. Development of a Cambridge Structural Database Subset: A Collection of Metal–Organic Frameworks for Past, Present, and Future. *Chemistry of Materials*, 29(7):2618–2625, 2017.

[45] R. E. Morris and P. S. Wheatley. Gas storage in nanoporous materials. *Angewandte Chemie International Edition*, 47(27):4966–4981, 2008.

[46] S. J. L. P. Martinez-Bulit, A. J. Stirk. Rotors, motors, and machines inside metal-organic frameworks. *Trends in Chemistry*, 2019.

[47] P. Reddy, E. M. Sevick, and D. R. Williams. Triangular cyclic rotaxanes: Size, fluctuations, and switching properties. *Proceedings of the National Academy of Sciences*, 115(38):9367–9372, 2018.

[48] A. Schneemann, V. Bon, I. Schwedler, I. Senkovska, S. Kaskel, and R. A. Fischer. Flexible metal–organic frameworks. *Chemical Society Reviews*, 43(16):6062–6096, 2014.

[49] C. Serre, F. Millange, C. Thouvenot, M. Noguès, G. Marsolier, D. Louër, and G. Férey. Very Large Breathing Effect in the First Nanoporous Chromium (III)-Based Solids: MIL-53 or Cr^{III} (OH)· $\{O_2C$-C_6H_4-$CO_2\}$ ·$\{HO_2C$-C_6H_4-$CO_2H\}_x$· H_2O_y. *Journal of the American Chemical Society*, 124(45):13519–13526, 2002.

[50] E. M. Sevick and D. Williams. Piston-rotaxanes as molecular shock absorbers. *Langmuir*, 26(8):5864–5868, 2010.

[51] E. M. Sevick and D. R. Williams. A piston-rotaxane with two potential stripes: Force transitions and yield stresses. *Molecules*, 18(11):13398–13409, 2013.

[52] E. M. Sevick and D. R. Williams. Conformational isomers of linear rotaxanes. *The Journal of Chemical Physics*, 141(11):114904, 2014.

[53] E. M. Sevick and D. R. Williams. A two-stroke, two-cylinder piston rotaxane motor. *ChemPhysChem*, 17(12):1927–1933, 2016.

[54] C. M. Simon, E. Braun, C. Carraro, and B. Smit. Statistical mechanical model of gas adsorption in porous crystals with dynamic moieties. *Proceedings of the National Academy of Sciences*, 114(3):E287–E296, 2017.

[55] J. F. Stoddart. The chemistry of the mechanical bond. *Chemical Society Reviews*, 38(6):1802–1820, 2009.

[56] H. Swenson and N. P. Stadie. Langmuir's theory of adsorption: A centennial review. *Langmuir*, 35(16):5409–5426, 2019.

[57] A. Torres-Knoop, A. Poursaeidesfahani, T. J. Vlugt, and D. Dubbeldam. Behavior of the enthalpy of adsorption in nanoporous materials close to saturation conditions. *Journal of Chemical Theory and Computation*, 13(7):3326–3339, 2017.

[58] C. Triguero, F.-X. Coudert, A. Boutin, A. H. Fuchs, and A. V. Neimark. Mechanism of breathing transitions in metal–organic frameworks. *The Journal of Physical Chemistry Letters*, 2(16):2033–2037, 2011.

[59] V. N. Vukotic and S. J. Loeb. Coordination polymers containing rotaxane linkers. *Chemical Society Reviews*, 41(18):5896–5906, 2012.

[60] V. N. Vukotic, C. A. O'Keefe, K. Zhu, K. J. Harris, C. To, R. W. Schurko, and S. J. Loeb. Mechanically interlocked linkers inside metal–organic frameworks: effect of ring size on rotational dynamics. *Journal of the American Chemical Society*, 137(30):9643–9651, 2015.

[61] E. B. Winston, P. J. Lowell, J. Vacek, J. Chocholoušová, J. Michl, and J. C. Price. Dipolar molecular rotors in the metal–organic framework crystal irmof-2. *Physical Chemistry Chemical Physics*, 10(34):5188–5191, 2008.

[62] M. Xue, Y. Yang, X. Chi, X. Yan, and F. Huang. Development of pseudorotaxanes and rotaxanes: from synthesis to stimuli-responsive motions to applications. *Chemical Reviews*, 115(15):7398–7501, 2015.

[63] O. M. Yaghi, M. O'Keeffe, N. W. Ockwig, H. K. Chae, M. Eddaoudi, and J. Kim. Reticular synthesis and the design of new materials. *Nature*, 423(6941):705–714, 2003.

[64] F.-Y. Yi, D. Chen, M.-K. Wu, L. Han, and H.-L. Jiang. Chemical sensors based on metal–organic frameworks. *ChemPlusChem*, 81(8):675–690, 2016.

[65] K. Zhu, C. A. O'Keefe, V. N. Vukotic, R. W. Schurko, and S. J. Loeb. A molecular shuttle that operates inside a metal–organic framework. *Nature Chemistry*, 7(6):514–519, 2015.

[66] K. Zhu, V. N. Vukotic, C. A. O'Keefe, R. W. Schurko, and S. J. Loeb. Metal–organic frameworks with mechanically interlocked pillars: controlling ring dynamics in the solid-state via a reversible phase change. *Journal of the American Chemical Society*, 136(20):7403–7409, 2014.

The Julia code to reproduce all plots in this thesis is available at:
github.com/SimonEnsemble/MORF*model*.